Accepted Manuscript

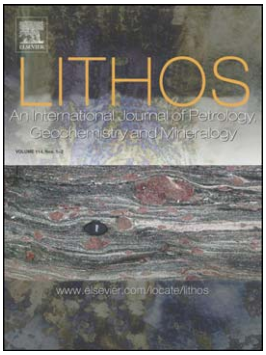

Cenozoic exhumation of the internal Zagros: first constraints from low-temperature thermochronology and implications for the build-up of the Iranian plateau

T. François, P. Agard, M. Bernet, B. Meyer, S.-L. Chung, M.H. Zarrinkoub, E. Burov, P. Monié

PII: S0024-4937(14)00258-8
DOI: doi: 10.1016/j.lithos.2014.07.021
Reference: LITHOS 3349

To appear in: *LITHOS*

Received date: 1 February 2014
Revised date: 14 July 2014
Accepted date: 21 July 2014

Please cite this article as: François, T., Agard, P., Bernet, M., Meyer, B., Chung, S.-L., Zarrinkoub, M.H., Burov, E., Monié, P., Cenozoic exhumation of the internal Zagros: first constraints from low-temperature thermochronology and implications for the build-up of the Iranian plateau, *LITHOS* (2014), doi: 10.1016/j.lithos.2014.07.021

This is a PDF file of an unedited manuscript that has been accepted for publication. As a service to our customers we are providing this early version of the manuscript. The manuscript will undergo copyediting, typesetting, and review of the resulting proof before it is published in its final form. Please note that during the production process errors may be discovered which could affect the content, and all legal disclaimers that apply to the journal pertain.

ACCEPTED MANUSCRIPT

Cenozoic exhumation of the internal Zagros: first constraints from low-temperature thermochronology and implications for the build-up of the Iranian plateau

T. François[1,2,*], P. Agard[1,2,3], M. Bernet[4], B. Meyer[1,2], S.-L. Chung[5], M.H. Zarrinkoub[6], E. Burov[1,2], P. Monié[7]

[1]Sorbonne Universités, UPMC Univ Paris06, ISTEP, Institut des Sciences de la Terre de Paris, France,

[2]CNRS, Centre National de la Recherche Scientifique, UMR 7193, Paris, France

[3]Institut Universitaire de France, IUF, Paris, France

[4]Institut des Sciences de la Terre (ISTerre), Université Joseph Fourier, Centre National de la Recherche Scientifique (CNRS), UMR 5275, F-38041 Grenoble, France

[5]Department of Geosciences, National Taiwan University, Taipei, 106, Taiwan

[6]Department of Geology, University of Birjand, Birjand, Iran

[7]Géosciences Montpellier, UMR 5243, 349095 Montpellier, France

* corresponding author: T.O.J.B.Francois@uu.nl

ACCEPTED MANUSCRIPT

Abstract

The Iranian plateau is a flat ~1.5-2 km high plateau thought to result from the collision between the Arabian and Eurasian plates since ~30 ± 5 Ma, and may represent a young analogue to the so far better studied Tibetan plateau. In order to constrain the exhumation history of the internal Zagros and of the Iranian plateau, we herein present apatite (U-Th)/He (AHe) and apatite (AFT) and zircon fission-track (ZFT) data on plutonic rocks from the Sanandaj-Sirjan Zone (SSZ), Urumieh-Doktar magmatic arc (UDMA), Central Iran and Kopet Dagh. Thermochronologic data show that the SSZ was exhumed early in the collision process (essentially before 25-20 Ma), with a likely acceleration of cooling during the late Eocene, from 0.04 to 0.3 mm/yr. Results suggest that cooling of the internal Zagros migrated from the SSZ to the UDMA during a more mature stage of the continental collision, after ~17 Ma (i.e., coeval with the outward propagation of deformation and topography fronts in the external Zagros). Constant exhumation rates in the UDMA (~0.3 mm/yr) suggest that no significant variation of erosion rates occurred since the onset of continental collision. In Central Iran, the overlap of ZFT, AFT and AHe ages from gneissic samples points to rapid cooling during the late Eocene (~42°C/Myr), which is consistent with previous reports on the formation of Eocene metamorphic core-complexes.

Keywords: Iranian Plateau; internal Zagros; exhumation; thermochronology; cooling rates; differential topography

ACCEPTED MANUSCRIPT

1 Introduction

The Zagros orogen marks ongoing collision of the northern edge of Arabia with Eurasia, following closure of the Neotethyan Ocean (e.g., Dercourt et al., 1986; Stampfli and Borel, 2002; Agard et al., 2011; Jackson, 2011). The timing of ocean closure and the initiation of collision has long been controversial, ranging from Late Cretaceous (Berberian & King, 1981) to Miocene (Berberian & Berberian, 1981) or uppermost Pliocene (Stöcklin, 1968). There is nevertheless a growing body of evidence in support of a Late Eocene to Oligocene initiation of collision at 30 ± 5 Ma (e.g., Jolivet and Faccenna, 2000; Agard et al., 2005; Vincent et al., 2005; Ballato et al., 2010; McQuarrie and van Hinsbergen, 2013).

The Zagros is consequently regarded as a young analogue to the Himalayan orogen (e.g., Hatzfeld and Molnar, 2010), where collision started at 50-55 Ma (Patriat and Achache, 1984) and the amount of shortening was much greater (e.g., Guillot et al., 2003). The formation of the Tibetan plateau is still controversial (e.g. Molnar et al., 1993; Meyer et al., 1998; Tapponnier et al., 2001; Hatzfeld and Molnar; 2010), but it is characterized by a significantly higher mean elevation (5000 m) than the Iranian plateau (1500 m). Recent studies, however, indicate that a ~3000 m high proto-Himalayan plateau (i.e., about one third of the current plateau area) already existed during the early stages of continental collision (Liu-Zeng et al., 2008; Van der Beek et al., 2009), suggesting that the present-day Tibetan plateau probably developed from the core (proto-plateau) to the outer parts of the orogen (Royden et al., 1997; Tapponnier et al., 2001; Liu-Zeng et al., 2008; Rohrmann et al., 2012).

Despite numerous recent studies on the Zagros (see reviews by Hatzfeld and Molnar, 2010; Agard et al., 2011; Jackson, 2011; Mouthereau et al., 2012), the topographic

ACCEPTED MANUSCRIPT

evolution of the Iranian plateau (and of the Zagros) remains largely unknown. Low-temperature thermochronology studies on the external Zagros (Gavillot et al., 2010; Hessami et al., 2001; Homke et al., 2010; Khadivi et al., 2012) demonstrated a progressive outboard migration of deformation (Fig. 1, inset) from the Crush zone (20-15 Ma) to the High Zagros (10 Ma) and the Zagros fold and thrust belt (5-0 Ma). Yet key questions remain unanswered: did plateau uplift start at the onset of collision, from the past 20 Ma onward (e.g., Meyer et al., 2006), or during the past 10-5 Ma only (Allen et al., 2004; 2011; Molinaro et al., 2005b; Mouthereau et al., 2012)? Did uplift occur rapidly or progressively? How was deformation on the upper Eurasian plate partitioned in space and time, and what are the causes of plateau formation?

In order to constrain the exhumation history of the Iranian plateau and contribute to the debate, we herein focus on the time record of cooling and exhumation in the internal Zagros using apatite (U-Th)/He, apatite and zircon fission-track data. The cooling history, in combination with structural and petrologic data, can provide useful information on the deformation of the Eurasian plate and contribute to the discussion of the formation of the plateau. This study is based on extensive sampling across Iran (Chiu et al., 2010). The results are afterwards discussed in the framework of regional tectonics.

2. Geological background

2.1. Structural organisation of the Zagros orogen

The Zagros orogen extends from the Turkish-Iranian border in the NW to the Makran area in the SE, where oceanic subduction is still active (e.g., Ellouz-Zimmermann et al., 2007). The Zagros fold and thrust belt proper essentially formed at the expense of

ACCEPTED MANUSCRIPT

the shortened margin of the Arabian Plate, whereas the Iranian plateau located to the north and to the east of the Zagros mountains corresponds to deformed continental blocks welded to Eurasia well before the Zagros collision. The Zagros orogen is conventionally divided by the Main Zagros Thrust (MZT) into the internal and external Zagros. The MZT marks the boundary between the Arabian lower plate and the Eurasian upper plate (Agard et al., 2005).

2.1.1. External Zagros

The external zone can be divided on the basis of sedimentary basins, deformation styles and seismic characteristics (Stöcklin, 1968; Alavi, 1980; Berberian and King, 1981; Berberian 1995, Lacombe et al., 2006; Mouthereau et al., 2006), into the Zagros Simply folded belt (ZFB; Fig. 1) and the High Zagros (HZ). The ZFB belt corresponds to an active accretionary wedge and is characterized by NW-SE trending folds of the 13 km thick EO-Cambrian to Quaternary sedimentary cover, detached from the Cambrian Hormuz salt (Hessami et al., 2001; Blanc et al., 2003; McQuarrie, 2004). The HZ is formed by Mesozoic carbonate rocks overthrusted by the Crush zone (i.e., radiolarite series and ultramafic bodies of the Neyriz ophiolitic complex) and characterized by larger offsets on basement faults, steep contacts and more ductile deformation (Ricou et al., 1977; Mouthereau et al., 2007b).

The internal Zagros comprises the following sub-parallel tectonostratigraphic domains, from SW to NE: the Sanandaj-Sirjan Zone (SSZ), the Urumieh-Dokhtar Magmatic Arc (UDMA) and Central Iran.

ACCEPTED MANUSCRIPT

2.1.2. The Sanandaj-Sirjan Zone (SSZ)

The Sanandaj-Sirjan Zone is immediately located to the north of the MZT and consists mainly of Permian to Jurassic interbedded phyllites and metavolcanics rocks showing a moderate metamorphic imprint (i.e., mostly low-grade greenschist facies rocks, with scarce amphibolites exhumed near some plutons; Agard et al. 2005). During the Middle Jurassic and Lower Cretaceous times, the SSZ represented an active Andean-like type margin whose calc-alkaline magmatic activity shifted briefly to the SW in the present-day Crush zone (Agard et al., 2011; Whitechurch et al., 2013), before shifting northward to the UDMA (Berberian and King, 1981; Sengör, 1990). By contrast to adjacent domains, the SSZ lacks marine Upper Oligocene-Lower Miocene sediments (Qom Formation; see below), which indicates that it was above sea-level at this time.

2.1.3. Urumieh Dokhtar Magmatic Arc (UDMA)

The UDMA (Schröder, 1944) is situated between the SSZ and Central Iran and runs parallel to the Zagros and the SSZ (Fig. 1). It forms a topographic ridge separating the SSZ from Central Iran, and bears in places >10 km thick volcano-sedimentary deposits (Dimitrijevic, 1973). The distinction between the SSZ and UDMA is justified by the emplacement of a subduction-related, mostly Eocene to Oligocene magmatic arc in the UDMA (Berberian and Berberian, 1981; Shahabpour, 2005; Chiu et al., 2013). However, the former Mesozoic calc-alkaline plutons found in the UDMA were emplaced in the Eurasian upper plate and should therefore be considered as part of the SSZ magmatic arc. Eocene volcanic rocks are composed of voluminous tholeiitic, calc-alkaline and K-rich alkaline magmatic rocks. Intrusive rocks are dominantly Oligo-Miocene (Berberian and Berberian, 1981). Magmatism resumed in Plio-

ACCEPTED MANUSCRIPT

Pleistocene times, with the onset of a restricted adakitic province (Jahangiri, 2007; Omrani et al., 2008; Chiu et al., 2013) suggesting a possible modification of geothermal gradients. This modification was tentatively related to slab break-off (Omrani et al., 2008) or lithospheric delamination (Hatzfeld and Molnar, 2010) beneath the Iranian Plateau.

2.1.4. Central Iran and Iranian plateau

The Central Iran comprises Precambrian basement rocks with metamorphic successions and plutonic suites (e.g. Chapedony and Posht-e-Badam complexes: Haghipour, 1974; Nadimi, 2007; Berberian and Berberian, 1981) overlain by Jurassic–Cretaceous and subordinate Palaeogene cover formations. A stage of extensional tectonic activity, marked by distributed extension and the formation of core-complexes, took place during mid-Eocene to Oligocene times (ca. 45-30 Ma; Verdel et al., 2007, Kargaranbafghi et al., 2012) and pre-dates later, syn- to post-Oligocene SW–NE shortening (Kargaranbafghi et al., 2010).

Whether Central Iran represents one coherent block (Stöcklin, 1968) or consists of a mosaic of microblocks (e.g. Lut, Tabas, Yazd and Anarak blocks) is debated. Despite complexities inherited from pre-Pan-African times, such as the N–S trend in the Tabas area, or the Lut 'block', which was a Precambrian basement horst (Stöcklin, 1968; Nadimi, 2007 and references therein), or the Palaeo-Tethys closure (Bagheri and Stampfli, 2008), the Central Iran, the UDMA and the SSZ together can be considered to represent the upper plate domain during most of the recent convergence history leading to the Zagros orogeny (Agard et al., 2011).

ACCEPTED MANUSCRIPT

2.2. Sedimentary constraints on the topographic evolution

The timing of plateau uplift can be partly constrained by stratigraphic records in Central Iran. The Central Iranian basins located on the overriding Eurasian plate are composed of two sub-basins, the Saveh-Qom area basin and the Great Kavir desert (Gansser, 1955a; Jackson et al., 1990; Morley et al., 2009 for a stragraphic review). The stratigraphic record from the Central Iranian basin shows that a large part of the Iranian plateau was overlain by a sequence of Upper Oligocene-Lower Miocene carbonate sedimentary rocks (Morley et al., 2009; Reuter et al., 2009). The Qom Formation (23-17 Ma) is approximately equivalent in time to the external Zagros Asmari Formation and is interpreted as an isolated, shallow seaway north of the Tethyan ocean (Harzhauser and Piller, 2007). The Aquitano-Burdigalian limestone of the Qom Formation is typically 500–1000 m thick and interbedded with clastic-dominated units of the Lower Red Formation and the Upper Red Formation (Gansser, 1955a; Morley et al., 2009). The base of the Upper Red Formation is a 400 m thick evaporitic unit with interbedded clastic rocks (Abaie et al., 1964). This thick unit can be interpreted as a progressive transition from marine to continental sedimentation and as a marker of surface uplift (Morley et al., 2009) or relative sea level fall.

This stratigraphy implies that the Central Iranian plateau area subsided under sea level during the Upper Oligocene - Lower Miocene (Qom Formation). The gradual transition between marine to continental sedimentation suggests that the Central Iranian plateau was for the last time at sea level during the Burdigalian and constrains the initiation of (at least part of the) plateau uplift to < 17 Ma.

In the Alborz Mountains (Fig. 1), the transition from shallow marine to continental sediments occurred after 36 Ma and marks the transition from extension to compression (Ballato et al., 2011). On the plateau south of the Alborz Mountains,

ACCEPTED MANUSCRIPT

Morley et al., (2009) estimated from balanced cross sections that the inversion of the intra-continental basins located between the Zagros and Alborz occurred during the Early Miocene or later, and was accompanied by 38 km of shortening, while Mouthereau et al. (2012) give an estimate of ~50 km.

3. Materials and Methods

Erosional exhumation is herein inferred from the cooling histories of Permian and Jurassic intrusive bodies, using zircon fission-track (ZFT), apatite fission-track (AFT), and (U-Th)/He (AHe) thermochronologic data.

3.1. Sampling strategy

To assess the timing and history of plateau exhumation, 15 plutonic samples from the upper plate internal domains, that U/Pb crystallization ages were already available (Chiu et al., 2010), were selected. AHe, AFT and ZFT analyses were performed on samples coming from the different sub-parallel tectonostratigraphic domains (with an s, u, c or k suffix for samples from the SSZ, UDMA, Central Iran and Kopet Dagh, respectively). The samples were collected from a wide range of lithologies (from leucogranites to gabbros), and zircon U-Pb crystallization ages (from 218 Ma to 5.4 Ma; Table 1; Fig. 1b). They comprise:

- one leucogranitic (09-13s) and one granitic (08-27) sample from Jurassic rocks in the SSZ, (~165 Ma; Chiu et al., 2010) which were selected to gain information on the pre-collision cooling of the Zagros belt,

- three granitic samples (08-14u, 08-31u and 10-60u), one gabbroic sample (10-61u), one dioritic sample (10-72u), one microdioritic sample (10-76u) and three

ACCEPTED MANUSCRIPT

granodioritic samples (10-79u, 10-80u and 10-106u) collected from rocks in the UDMA which have zircon U-Pb ages between 175.2 Ma and 5.4 Ma (Chiu et al., 2010). Samples 08-14u and 10-60u were taken from the extended northern part of the SSZ.

- one granitic (08-09c) and one gneissic (08-10c) sample were collected from Eocene rocks (~45 Ma; Chiu et al., 2010) from Central Iran,
- one granodioritic (09-01k) and one dioritic (09-03k) sample from Kopet Dagh, to provide reference anchor points far from to the Neotethyan suture zone.

3.2. Analytical techniques

3.2.1. Apatite (U-Th)/He (AHe)

(U-Th)/He age determinations were carried out at the laboratory Géosciences Montpellier, Université Montpellier II (France). Inclusion-free apatite grains were handpicked from sample aliquots, individually loaded in Pt tubes and laser heated for 10 min at 950°C together with several aliquots of Durango apatite age standard for calibration. The gas released was spiked with ^{3}He and purified using cold Zr-Al getters and a cryogenic trap. Helium was analyzed on a quadruple mass-spectrometer. For some grains, a re-heating cycle was applied in order to ensure the complete helium release. In this case, the amount of helium released remains similar to the blank value measured between each sample. After laser heating, apatites were spiked using an enriched ^{235}U-^{230}Th tracer and dissolved in HNO_3. U and Th concentrations were determined by isotope dilution ICP-MS analysis. Mean (U-Th)/He ages were calculated on the basis of 2-4 replicate analyses (i.e. different apatites grains). After blank corrections, all ages were calculated using standard α–ejection corrections (Farley et al., 1996; Farley 2000). All AHe ages were obtained from four aliquots,

ACCEPTED MANUSCRIPT

except for sample 08-27s for which only two aliquots were analyzed (Table 2; Figs. 3a, 4a). Because apatite grain size strongly influences the (U-Th)/He age, aliquots with crystals larger than 60 μm and devoid of inclusions were chosen for analysis (Reiners and Farley, 2001).

3.2.2. Apatite (AFT) and zircon (ZFT) fission track

Sample preparation and analyses were performed in the Institut des Sciences de la Terre (ISTerre), Université Joseph Fournier, in Grenoble (France). Apatite and zircon grains were separated from crushed rocks using standard sieving, heavy liquid and magnetic separation techniques. Apatite grains were mounted in epoxy resin and zircons in PFA Teflon®. Mounted samples were then polished to expose internal grain surfaces. Apatite samples were etched in 5.5-mol HNO_3 at 21°C for 20s to reveal spontaneous tracks. Zircons concentrates were etched in a NaOH-KOH melt at 230°C between 5 and 40h. Apatite and zircon samples were irradiated separately in the FRM II reactor, Munich, Germany. Thermal neutron fluence was monitored using IRMM540R dosimeter glasses for apatite and corning CN-1 dosimeter glasses for zircon. The external detector method with muscovite sheets was used for analysis (Gleadow, 1981; Hurford and Green, 1982). The muscovite detectors were etched after irradiation at 20°C in 48% HF for 18 min. Spontaneous and induced fission tracks were counted dry on an Olympus BH2 optical microscope at ×1250 magnification, using the FTStage 4.04 system of T. Dumitru. Central ages (Galbraith and Laslett, 1993) have been calculated with the zeta calibration method (Hurford and Green, 1982), using Durango (31.3 ± 0.3 Ma, Naeser and Fleischer, 1975) and Fish Canyon Tuff (27.8 ± 0.2 Ma, Hurford and Hammerschmidt, 1985) age standards for apatite, and Fish Canyon Tuff and Buluk Tuff (16.2 Ma) age standards for zircon.

ACCEPTED MANUSCRIPT

Conventionally, the range of effective closure temperatures for the different thermochronologic systems depends on cooling rate, chemical compostition, crystal size and/or accumulated radiation damage (e.g. see Dodson 1973; Brandon et al., 1998; Reiners and Brandon, 2006; Bernet, 2009). The closure temperatures for a common orogenic cooling rate of about 15°C/Myr and average chemical composition or radiation damage are ~75±5°C for AHe (Farley 2000); ~110±10°C for AFT (Brandon et al., 1998) and ~240±20°C for ZFT (Hurford, 1986; Brandon et al., 1998; Bernet, 2009). The effective closure temperatures for the different dating techniques and the different samples were therefore estimated iteratively for each cooling path using the *Closure program* (M.Brandon).

3.3. Geological significance of cooling ages

U/Pb ages correspond to the age of zircon crystallization in a magma (at T~800°C; Cherniak and Watson, 2000), whereas in the case of monotonic cooling ZFT/AFT/AHe ages mark the crossing of isotherms at approximately 240°C, 110°C and 75°C (see above). Cooling histories of intrusive bodies, depend on their volume, shape, and emplacement depth, which is generally difficult to determine.

The interpretation of pluton cooling ages must be treated with caution. For example, the case where ZFT, AFT and AHe ages overlap may indicate rapid post-magmatic cooling of the plutonic intrusion either because of shallow emplacement, or very rapid exhumation (cases 1 and 2; Fig. 2a), or a combination of both. Similarly, without further thermochronologic information it is difficult to determine early exhumation rates from ZFT cooling age alone if post-magmatic cooling was slow (i.e., when the U/Pb and ZFT ages differ; case 3, Fig. 2a), because the exact emplacement depth is not known, and it is not clear how much cooling was caused by erosion and how

ACCEPTED MANUSCRIPT

much by post-magmatic relaxation of isotherms.

Numerical simulations and geophysical observations (e.g. Kukowski and Neugebauer, 1990; Weinberg and Podlachikov, 1994; Petford et al., 2000; Burov et al., 2003), show that if a pluton is emplaced at depths where T exceeds 350°C (i.e., ~ 5 or 10 km, assuming geothermal gradients of 60 or 30 °C/km, respectively), post-magmatic cooling takes less than 1 Ma. Assuming that the coldest possible emplacement temperature was ~350°C (without tectonic activity) thus only provides a minimum early erosional exhumation rate for these cases (Fig. 2b, case 3).

To overcome these limitations, the use of mineral pair analyses FT or He on apatite and zircon is essential to constrain the cooling history and in particular discern between exhumation and post-magmatic cooling of plutons. Finally, we recall in Figure 2b that surface uplift (and therefore topography) is equal to rock uplift minus exhumation (e.g., England and Molnar, 1990): cooling paths inferred from thermochronologic ages (in this case history between the ZFT and AHe closure temperature) thus chiefly inform on exhumation.

4. Results

4.1. AHe, AFT and ZFT results

Apparent cooling ages of all three dating techniques are reported as pooled ages with ±2σ uncertainties in Tables 2, 3 and 4.

AHe ages range from 53.03 ± 0.7 Ma (08-09s) to 6.08 ± 0.31 Ma (10-61u). Younger AHe ages are found along the UDMA (Figs. 3a, 4), and show a cluster of Late Miocene ages (6-7 Ma), particularly in the southeastern part of the UDMA.

Except for sample 10-80u for ZFT, all FT analyses showed a $P(\chi^2)$ >5%,

ACCEPTED MANUSCRIPT

indicating a single cooling age distribution for each sample, with no indication of partial resetting. Fission-track ages were calculated with the BINOMFIT software of Brandon (see Brandon 1996, Stewart and Brandon 2004) with about 10-30 grains analyzed per AFT and ZFT sample.

AFT ages show a range from 49.8 to 4.7 Ma throughout the study area (Table 3). The oldest age (49.8 ± 4.8 Ma) is found in the northwestern part of the SSZ. The youngest ages (between 20 and 4.7 Ma) are found along the UDMA (Table 3, Figs. 3b, 4a). For the younger samples (Table 3), the small number of induced and spontaneous fission tracks, which also relates to the low concentration of uranium in apatite, leads to greater uncertainties on age determinations.

The ZFT ages show an even greater range of cooling ages, between 141.7 to 5.5 Ma (Table 4, Figs 3c and 4a). We distinguish one age group composed of the oldest ZFT ages, in the SSZ (08-27s: 141.7 ± 26 Ma), the Kopet Dagh (09-03k: 126.7 ± 30 Ma) and one sample in the UDMA (08-14u: 121 ± 17 Ma). Other ages are distributed between 66.7 and 5.5 Ma with the youngest age, again, in the UDMA (10-76u: 5.5 ± 0.7 Ma). Within error, cooling ages for each sample yield consistent ZFT > AFT > AHe ages (Fig. 4). Nevertheless, some of the reported samples show an apatite AHe ages older than their AFT ages. This discrepancy between the two thermochronologic methods could be linked to the degree of accumulated radiation damage within the crystal lattice and/or by the assimilation of ejected He. (see for example, Green and Duddy, 2006; Green et al., 2006).

Some samples (e.g. samples 10-76u, 10-79u and 10-80u) show similar AHe, AFT ZFT and U/Pb ages. Interpretation of these samples is typically ambiguous (i.e., shallow emplacement or fast exhumation, as noted in 3.3; cases 1 and 2; Fig. 2a) and they cannot be used in the interpretation of the exhumation history of the Iranian

ACCEPTED MANUSCRIPT

plateau (see chapter 5.1.).

4.2. Results vs. tectonic domains

Cooling rates can be calculated by dividing the temperature difference between the closure temperatures of two radiometric systems divided by the difference in cooling ages obtained for each system. Cooling ages are translated in terms of exhumation rates and then estimated assuming a geothermal gradient of 30 °C/km, typical of continental arc terranes (see discussion) and a mean surface paleo-surface temperature of 15°C.

4.2.1. Sanandaj Sirjan Zone

The two granitic SSZ samples 09-13s and 08-27s were emplaced coevally, as indicated by their U/Pb ages of 165±2 Ma (Table 1). Both granites cooling path can be interpreted as a slow exhumation during the Mesozoic (Fig. 4a). This early exhumation was probably slightly faster for sample 08-27s, located in the central part of the SSZ, than for sample 09-13s located further to the NW (Fig. 4a). However, the slope of the cooling path between U/Pb to ZFT ages only provides an upper bound on the exhumation rate, as the exact emplacement depth of the pluton is unknown. If, for example, sample 08-27s was emplaced at depths corresponding to T ~350°C (see section 3.3), the exhumation rate could be the same as the one calculated for sample 09-13s (Fig. 4a).

Both samples evidence a later, Cenozoic increase in exhumation rate, although somewhat differently (Fig. 4a). Sample 08-27s experienced rapid cooling during the Eocene, whereas sample 09-13s shows less increase cooling during the late Eocene to Oligocene period, which coincides with the onset of collision. Assuming a paleo-

ACCEPTED MANUSCRIPT

geothermal gradient of 30°C/km, these samples underwent a minimum exhumation of ~11 km since 165 Ma. Average long-term erosional exhumation rates are 0.04 ± 0.014 mm/yr during the Mesozoic and 0.31 ± 0.11 mm/yr during the upper Eocene-Oligocene. The assertion that rocks of the SSZ samples had reached shallow crustal depths (< ~2-3 km) by the late Oligocene is further supported by the AFT cooling ages of 26 Ma and 27 Ma reported from other SSZ samples (Omrani 2008, unpublished data and Homke et al., 2010 respectively).

4.2.2. Urumieh Dokhtar Magmatic Arc

UDMA samples can be split into three different cooling age groups (Fig. 4b). In the first group, samples 10-60u and 08-14u show an identical cooling path to those of the SSZ samples (0.04 ± 0.011 mm/yr) from Mesozoic to Eocene (Fig. 4b).

The second group includes samples 10-61u, 10-72u, 08-31u and 10-106u, which all crystallized prior to 15 Ma (Fig. 4b). They yield total exhumation rate estimates of ~4.6 km in ~43 Myr (between 49.2 Ma (ZFT) and 6.08 Ma (AHe)), ~6 km in ~20 Myr (between 26.8 Ma (ZFT) and 7.25 Ma (AHe)), ~1.7 km in ~6.7 Myr (between 19.8 Ma (AFT) and 13.09 Ma (AHe)), and ~1.7 km in ~5.8 Myr (between 12.3 Ma (AFT) and 6.47 Ma (AHe)) respectively, which corresponds to exhumation rates of 0.12 ±0.02 mm/yr, 0.31±0.05 mm/yr, 0.25±0.04 mm/yr and 0.29±0.1 mm/yr, respectively. Despite differences in age and structural setting, the three last samples (10-72u, 08-31u, 10-106u) are thus characterized by similar Neogene exhumation rates (~0.28 ± 0.06 mm/yr) since the Early Miocene.

The third group is composed of the southeastern samples 10-76u, 10-79u and10-80u and shows a tight cluster of young cooling ages, between 9 and 6 Ma, for all thermochronometric systems. Sample 10-76u is in fact a subvolcanic microdiorite,

ACCEPTED MANUSCRIPT

and the petrologic characteristics of the granodiorite samples 10-79u and 10-80u are consistent with emplacement at shallow (~2-3 km) crustal levels. Emplacement at ~2-3 km depth would imply a minimal rock uplift of ~2-3 km between 9 and 6 Ma and correspond to an exhumation rate of 0.39 ± 0.08 mm/yr.

4.2.3. Central Iran and Kopet Dagh

In Central Iran, the overlap (within error) of the ZFT, AFT and AHe ages from the gneissic sample (08-10c) points to fast cooling rate (~42°C/Myr) during the Late Eocene and Oligocene (Fig. 4c).

The two Kopet Dagh samples 09-01k and 09-03k have Triassic ages. One of them (09-01k) shows a slow Triassic to Eocene cooling path (Fig. 4c), which is similar to the cooling path of the SSZ and the oldest UDMA samples (08-14u and 10-60u). These results hint to the fact that Kopet Dagh samples were probably already exhumed to the near surface during the Eo-Oligocene, implying only minimal exhumation since ca. 30 Ma (max. 2-3km in 30 Myr; Figure 4c).

5. Discussion

5.1. Constraints on exhumation

Our thermochronological results provide constraints on cooling histories and exhumation (mainly driven by erosion in the absence of widespread extensional tectonics) of the internal Zagros since the early stages of Neotethys subduction. In the absence of constraints on past continental thermal gradients, exhumation rates estimated below rely on the assumption of an average value of 30°C/km. This hypothetical value, somewhat higher than the 15-25°C estimated for the external part

ACCEPTED MANUSCRIPT

of the Zagros (Mouthereau et al., 2006; Gavillot et al., 2010; Homke et al., 2010), is probably reasonable for internal zones such as the Mesozoic SSZ and Cenozoic UDMA magmatic arcs. Lower geothermal gradients would result in higher exhumation rates. For the sake of comparison, we also assumed a similar thermal gradient for samples from both the SSZ and the UDMA magmatic arcs, although the gradient may have been slightly higher for the UDMA given its volumetrically large Cenozoic magmatic activity (Berberian and Berberian 1981; Omrani et al., 2008).

We discuss below the detailed trajectories of key samples (i.e. with clearly different cooling ages especially between AFT and AHe ages) from the SSZ and UDMA (i.e., samples 08-27s, 09-13s and 08-14u, 08-31u, 10-61u, 10-72u, 10-106u respectively; Fig. 5a). The cooling paths of the SSZ and Kopet Dagh rocks are similar until at least 50-40 Ma and point to slow cooling (~2°C/Myr) and exhumation rates (~0.04 mm/yr) during oceanic subduction. The oldest UDMA samples (08-14u, 10-60u, 10-61u) emplaced in the upper plate prior to the differentiation of the SSZ and UDMA domains evidence similar slow exhumation (between 0.04 and 0.12 mm/yr).

Figure 5b places emphasis on the transition period from subduction to collision. Irrespective of their exact elevation, the cooling paths of these samples are shown between 50 and 0 Ma, with error envelopes incorporating all associated uncertainties (i.e., analytical standard deviations, ambiguities associated with early exhumation paths; see chapter 3.3).

In the central SSZ, sample 09-13s shows a transition from slower (~0.04 mm/yr) to faster (0.31 mm/yr) exhumation since the late Eocene (~39.6 ± 6.5 Ma). This acceleration of exhumation broadly coincides with the onset of collision between the Arabian distal margin and Eurasia (Agard et al., 2005; i.e., initiation of “soft” continental collision; Ballato et al., 2011). This is consistent with the late Oligocene

ACCEPTED MANUSCRIPT

AFT ages (27 and 26 Ma; Fig.3) obtained by Homke et al. (2010) and Omrani (2008). AHe ages for the SSZ (22 and 53 Ma for samples 09-13s and 08-27s, respectively) indicate that there is no to only minimal erosion along the SSZ after the Oligocene. Besides, no Miocene Qom Formation was deposited on the deformed SSZ. The SSZ may thus already have formed a smooth, plateau-type topography by then. The absolute elevation of that plateau-type topography by that time remains nonetheless unknown.

Exhumation along the UMDA takes place at relatively constant rates of ~0.2 mm/yr throughout the Miocene (samples 08-31u, 10-61u, 10-72u, 10-106u; Fig. 5a), without evidence either of acceleration or deceleration. The particularly homogeneous AHe ages for the UDMA samples (i.e., all being at ~1.3 km depth by ~6 Ma) point to minimal exhumation rates of ~0.2 mm/yr. The similar U/Pb, ZFT, AFT and AHe ages of samples 10-76u, 10-79u and 10-80u indicate rapid cooling ($\geq$ 100 C°/Myr), most probably associated with shallow depth emplacement (i.e., 2-3 km max. as shown by their plutonic to sub-volvanic petrological textures), rather than with rapid exhumation. The latter alternative interpretation cannot be discarded, however, especially considering samples coming from the same area (Fig. 1) and where adakites (and possibly slab-breakoff) were reported (Omrani et al., 2008). We nevertheless note that the overlap of these cooling ages could also result from their very low U and He content (see samples with a star in Tables 3 and 4). More data is clearly required for this part of the UDMA.

In the eastern part of Central Iran, the rapid cooling at ~42°C/Myr of the gneissic sample 08-10c accords with the cooling of metamorphic core complexes during the Eocene noted by Verdel et al., (2007) and Karagaranbafghi et al. (2012), rather than to

ACCEPTED MANUSCRIPT

shallow emplacement. The AHe ages reported here are close to those of the latter study (Fig. 1).

The Inferred exhumation rates for the SSZ, UDMA and Central Iran samples are compared in figure 5b. The Central Iran samples are the only ones showing relatively fast exhumation (ie, > 1mm/yr). Importantly, no change in exhumation rates is observed in the SSZ and UDMA samples during the Miocene, despite the report of several tectonic events: (1) inversion of the Central Iranian basin, transition between extensional to compressional tectonics and onset of clastic sedimentation since the Burdigalian (Morley et al., 2009), (2) change in structural style in the Alborz Mountains at ~7-5 Ma (Axen et al 2001, Ballato et al., 2011, 2012), (3) slab-breakoff (Hafkenscheid et al., 2006; Omrani et al., 2008), (4) regional-scale plate-tectonic reorganization along the Arabia-Eurasia collision (Allen et al., 2011).

5.2. Exhumation history and implications for topographic build-up of the internal Zagros

Keeping in mind limitations associated with deriving exhumation rates from cooling histories (Reiners and Brandon 2006, Willet and Brandon; 2013), the above data allow proposing a tentative reconstruction of the exhumation history of the internal Zagros. These data also shed some light on the evolution of its relative topography during the Cenozoic (Fig 6).

Before ~40 Ma (Upper Eocene) the Neotethyan oceanic lithosphere is being subducted beneath Eurasia (since the upper Triassic: Berberian and King 1981; Arvin et al., 2007). We therefore interpret the slow cooling in the SSZ, UDMA and Kopet Dagh until ~40 Ma as reflecting very limited topography during oceanic subduction, in a similar fashion to the present-day oceanic subduction beneath Makran. By

ACCEPTED MANUSCRIPT

contrast, the acceleration of exhumation rate in one of the SSZ samples, from 0.04 to 0.31 mm/yr, may point to a change in erosion, and thus topography uplift, near the suture zone at the onset of collision.

We focus below on the (Late Oligocene to) Miocene evolution of the internal Zagros, after the onset of collision (i.e. 30 ± 5 Ma; Agard et al., 2011 and references therein; Fig. 6).

— 25-17 Ma: The presence of the 23-17 Ma, Early Miocene Qom Formation (coeval with the deposition of the Asmari Formation in the external Zagros) is an important milestone for exhumation and topographic build-up of the internal Zagros, showing that most of the UDMA and the Iranian plateau were at or near sea level for the last time at 17 Ma (Morley et al., 2009, Reuter et al., 2009), and that no erosion took place there during this period. No such Qom deposits are found in the SSZ. The late Oligocene AHe cooling age of sample 09-13s SSZ indicates that this rock was at ~1.5-2 km depth beneath the surface at 22 Ma. Assuming an exhumation rate of 0.24 mm/yr (i.e., the same as after the Eocene acceleration), this SSZ sample would have arrived at the surface at 16.5 Ma. This, together with the 53 Ma AHe age of sample 08-27s, points in any case to very low erosion rates in the SSZ over the last 20 My,

— 17-10 Ma: Exhumation velocities in the UDMA are around 0.2-0.3 mm/yr during that period (Fig. 5a,b), which coincides with the sedimentation of the lower part of the Upper Red formation made of coarse clastic deposits with a large volcanoclastic component derived from the UDMA. Although erosion in the SSZ is limited, some fragments are also derived from the SSZ (Morley et al., 2009). The extensive sedimentation of the Upper Red formation in both the UDMA and Central Iran points to the absence of a significant topographic step between these two areas (Figure 6b).

ACCEPTED MANUSCRIPT

The moderate ~0.2-0.3 mm/yr exhumation rates for samples adjacent to the Qom basin (08-31u and 10-106u) broadly fit with the sedimentation rate recorded in the Central Iranian basin (i.e., 0.6 mm/yr; ~7 km deposited between 17.5 and 6.2 Ma: Ballato et al., 2008; Morley et al., 2009), especially when taking into account additional sedimentary supply from the Alborz (where the exhumation rate is estimated between 0.025 and 0.23 mm/yr; Rezaeian et al., 2012). Note that average erosion rates for the UDMA would fall to 0.05-0.15 mm/yr assuming higher, back-arc type geothermal gradients (e.g., 50-60°C/km), hence quite lower than estimates from sedimentary fluxes.

— 10-0 Ma: At 6 Ma a surge in magmatic activity is observed in at least part of the UDMA (as shown by U/Pb ages of south-central UDMA). Thermochronological data also indicate that most UDMA samples still lie at 1.5-2 km beneath the surface (Figure 6d). Compressional deformation is recorded in the UDMA until ~3 Ma. By contrast with the lower part of Upper Red Formation, depocenters of the Late Upper Formation (10-7 Ma) are located between the uplifted UDMA massifs and the central Iranian basin.

We interpret this shift in sedimentation away from the UDMA as marking an increase in UDMA erosion and as the onset of a topographic step between the UDMA and Central Iran (Figure 6c). The respective contributions from shortening and magmatic production to the increased erosion (and differential topography) are unfortunately unknown at present.

After 3 Ma little sedimentation occurs in the Central Iranian Basin (Morley et al., 2009). This suggests that from 3 Ma onward the UDMA and Central Iran were likely jointly uplifted to their present day elevation (Figure 6f). This suggests, in turn, that a

ACCEPTED MANUSCRIPT

somewhat faster exhumation rate may have prevailed for the UDMA samples between 6 and 3 Ma.

We finally recall that thermochronological data and sedimentary constraints provide no clue on absolute elevations and that the general uplift of the entire internal Zagros may have taken place anytime, hence at an unknown rate, after 17 Ma.

5.3. Implications for Arabia-Eurasia convergence zone

These data, despite a relatively small number of samples, provide useful insights on the evolution of the Arabia-Eurasia convergence (Fig. 6):

(1) The similar, slow cooling paths of the SSZ, UDMA and Kopet Dagh samples during oceanic subduction (Fig. 5a) are consistent with the existence of a unique Central Iranian block, encompassing the SSZ, UDMA and Central Iran (Sengör 1984; Stampfli and Borel, 2002; Agard et al., 2011).

(2) Exhumation processes in the SSZ, hence within the first 100-150 km aside the suture zone, likely increased during the onset of continental collision (possibly as a result of increased coupling between the two plates).

(3) The locus of exhumation migrated inland towards the UDMA after ~17-10 Ma. This is broadly coeval with the outboard propagation of deformation in the external Zagros **(**Hessami et al., 2001; Allen et al., 2004; Omrani, 2008; Gavillot et al., 2010; Homke et al., 2010; Wrobel-Daveau, unpublished data 2011; Khadivi et al., 2012; Fig. 1). Relatively low exhumation rates across the UDMA (< 0.3 mm/yr) suggest that collision was accommodated in the upper plate by low-rate deformation. This timing is compatible with former suggestions of deformation in Central Iran (Morley et al., 2009) but may have started as early as 17 Ma (i.e., earlier than the 12 Ma proposed by Allen et al., 2004). This migration also coincides with a 35% decrease in the

ACCEPTED MANUSCRIPT

convergence rate (McQuarrie et al., 2003; Hatzfeld and Molnar, 2010; McQuarrie and van Hinsbergen, 2013) and with a shift from 'soft' to 'hard' collision (Ballato et al., 2011; Mouthereau et al., 2012), despite debates on reconstructed lengths of the stretched Arabian continental margin (e.g., Vergés et al., 2011 and references therein).

(4) Our results confirm the existence of an extensional tectonic episode in the upper plate during or slightly prior to the onset of collision. This change in the style of upper plate deformation was related to ablative subduction (Agard et al., 2011) or slab retreat (Moritz et al., 2006; Verdel et al., 2007), with both interpretations emphasizing the increase in slab bending after early collision of the distal Arabian margin.

(5) The timing and rate of uplift of the Iranian plateau is not known and not readily accessible with our data (as recalled in 5.2), yet inferences can be made on relative topography (Fig. 6):

— the onset of differential topographic between the UDMA and the Central Iranian basin dates back to between 10 and 6 Ma. This timing coincides with slab breakoff beneath the UDMA, supported by both geochemistry and seismic tomography (5-10 Ma; Omrani et al., 2008; Agard et al., 2011).

— erosion was, during the Mid-Miocene, located in the UDMA rather than in the SSZ.

While the formation of a large-scale plateau over Iran is probably best explained by the partial delamination and/or lithospheric mantle removal of the subcontinental Eurasian mantle (Hatzfeld and Molnar, 2010 ; François et al., 2014), these observations suggest that other processes such as slab breakoff or crustal shortening of the upper plate may have contributed to the build-up of differential topography on a smaller scale (i.e., typically 200-300 km or 50 km, respectively (van Huenen and Allen, 2011; Mouthereau et al., 2007b, 2012)).

ACCEPTED MANUSCRIPT

6. Conclusions

The combination of low-temperature thermochronology data (i.e., apatite (U-Th)/He, apatite and zircon fission-track dating) on a set of representative Iranian plutons is herein used to constrain the cooling paths and exhumation history of the internal Zagros. The data show that exhumation of the upper plate Sanandaj-Sirjan zone (SSZ) mainly took place prior to 25 Ma. Exhumation rates in the SSZ were slow (0.04 mm/yr) during oceanic subduction throughout most of the Mesozoic and increased to 0.3 mm/yr at the onset of collision (i.e., around 30±5 Ma). Exhumation across the Urumieh-Dokhtar magmatic arc (UDMA) mainly took place after 17 Ma, at similarly moderate denudation rates (0.2-0.3 mm/yr).

The results shown here also suggest that (1) the onset of collision resulted in an increase in elevation in the vicinity of the suture zone, (2) exhumation migrated to the NE (UDMA) after ~20 Ma, at the same time as towards the SW (external Zagros). This is consistent with the idea that a more mature collision induced a broadening of the orogen. The data also shed some light on the acquisition of differential topography but not on plateau uplift, which started after 17 Ma.

ACCEPTED MANUSCRIPT

Acknowledgments

This study has benefited from funding by the Institut des Sciences de la Terre de Paris (ISTEP, UPMC-CNRS INSU) and Institut Universitaire de France (IUF).

ACCEPTED MANUSCRIPT

ACCEPTED MANUSCRIPT

Figure captions

Figure 1.

Sampling locations:

a) Topographic map showing the main structures within the Arabia-Eurasian convergence zone and sample locations. Blue frames show available low temperature thermochronology data in the literature (data from, Axen et al., 2001; Omrani, unpub data, 2008; Verdel et al., 2007; Guest et al., 2006a; Gavillot et al., 2010; Homke et al., 2010; Karagaranbafghi et al., 2012; Khadivi et al., 2012; Wrobel-Daveau, unpub data, 2011; Ballato et al., 2012; Rezaeian et al., 2012. Black arrows indicate convergence rates of Arabia with respect to Eurasia (from Vernant et al., 2004). Inset: simplified structural map showing the extension of crustal thickening over the last 12 and 7 Myr across the Arabia-Eurasia collision, as suggested by Allen et al. (2004).

b) Ages of the selected plutonic samples (from Chiu et al., 2010; see Table 1 for details).

Figure 2.

a) Cartoon illustrating the various possible interpretations of cooling ages of plutons emplaced at different depths, assuming a constant geothermal gradient. In the first two cases, the overlap of ages is ambiguous and may indicate either shallow emplacement of the pluton (1) or rapid exhumation (2). In the third case, the different cooling ages reveal the effective exhumation and provide informative temperature-time paths

b) Cartoon recalling that surface uplift (dh) is equal to rock uplift (R. uplift) minus exhumation (i.e., erosion; England and Molnar 1990). Exhumation corresponds here to the net difference between (h2+Z2) and (h1+Z1), where h and Z are positive and

ACCEPTED MANUSCRIPT

negative, respectively.

Figure 3.

Low-temperature thermochronology data and location of calculated ages: **a)** AHe, **b)** AFT and **c)** ZFT. See caption of Figure 1 for references of published ages.

Figure 4.

a) Cooling paths for the SSZ, UDMA, Central Iran and Kopet Dagh. The closure temperature for each sample is calculated as a function of exhumation rate (see Reiners and Brandon, 2006). Dashed lines represents minimal exhumation rates (see § 3.3).

b) Cooling paths of key samples (see text). The depth range is calculated for a thermal geotherm of 30°/km. The age of the Qom Formation is indicated (Qom fm.) and Depth-time position of these key samples (irrespective of their exact elevation) at 50, 25, 20, 13 and 0 Ma. Error envelopes incorporate all associated uncertainties (i.e., analytical standard deviations, ambiguities associated with early exhumation paths; see chapter 3.3).

c) Evolution of exhumation rate between 50 and 0 Ma for the SSZ, UDMA and Central Iran. The number corresponds to the different stage of exhumation history subsequently shown in the Fig.5.

Figure 5.

Tentative relative topographic reconstruction over the last 50 Myr along a NE-SW traverse. Each time step is set against the evolution of the Arabia-Eurasia convergence (see text). The sedimentary record from the Central Iranian basin is schematized from

ACCEPTED MANUSCRIPT

Morley et al., (2009). The present day topography of Central Zagros is represented by the blue line in the panel 5.f (0 Ma).

Table 1: Sample locations, Rocks type and U/Pb Ages

Table 2: Analytical data for apatite (U-Th)/He age determination

Table 3: Apatite fission track analytical data. The stars represent the sample with low U concentration

Table 4: Zircon fission track analytical data. The stars represent the sample with low U concentration

ACCEPTED MANUSCRIPT

ACCEPTED MANUSCRIPT

References

Abaie, I., Ansari, J.J., Badakhshan, A., Jaafari, A., 1964. History and development of the Alborz and Sarajeh fields of central Iran. World Petroleum Congress Proceedings, Section II, Paper 13, PD3, p. 697–713.

Agard, P., Omrani, J., Jolivet, L., Mouthereau F., 2005. Convergence history across Zagros (Iran): Constraints from collisional and earlier deformation. Int. J. Earth Sci. 94, 401–419, doi:10.1007/s00531-005- 0481-4.

Agard, P., Omrani J., Jolivet, L., Whitechurch, H., Vrielynck, B., Spakman, W., Monié, P., Meyer B., Wortel R., 2011. Zagros orogeny: a subduction-dominated process. Geol. Mag. 148, issue 5-6, 689-691.

Alavi, M., 1980. Tectonostratigraphic evolution of the Zagrosides of Iran. Geology 8, 144-149.

Allen, M., Jackson, J.A., Walker, R., 2004. Late Cenozoic reorganization of the Arabia-Eurasia collision and the comparison of short-term and long-term deformation rates. Tectonics 23, doi:10.1029/2003TC001530.

Allen, M.B., Kheirkhah, M., Emami, M.H., Jones, S.J., 2011. Right-lateral shear across Iran and kinematic change in the Arabia–Eurasia collision zone. Geophys. J. Int. 184(2), 555-574.

Arvin, M., Pan, Y., Dargahi, S., Malekizadeh, A., Babaei, A., 2007. Petrochemistry of the Siah-Kuh granitoid stock southwest of Kerman, Iran: Implications for initiation of Neotethys subduction. J. Asian Earth Sci. 30(3), 474-489.

ACCEPTED MANUSCRIPT

Axen, G., Lam, P.S., Grove, M., Stockli, D.F., Hassanzadeh, J., 2001. Exhumation of the west central Alborz Mountains, Iran, Caspian subsidence, and collision-related tectonics. Geology 29, 6, 559-562.

Bagheri, S., Stampfli, G.M., 2008. The Anarak, Jandaq and Posht-e-Badam metamorphic complexes in central Iran: New geological data, relationships and tectonic implications. Tectonophysics 451(1-4), 123-155.

Ballato, P., Nowaczyk, N.R., Landgraf, A., Strecker, M.R., Friedrich, A., Tabatabaei, S.H., 2008. Tectonic control on sedimentary facies pattern and sediment accumulation rates in the Miocene foreland basin of the southern Alborz mountains, northern Iran. Tectonics 27, 6, doi :10.1029/2008TC002278.

Ballato, P., Mulch, A., Landgraf, A., Strecker, M.R., Dalconi, M.C., Friedrich, A., Tabatabaei, S.H., 2010. Middle to late Miocene Middle Eastern climate from stable oxygen and carbon isotope data, southern Alborz mountains, N Iran. Earth Planet. Sci. Lett. 300(1), 125-138.

Ballato, P., Uba, C.E., Landgraf, A., Strecker, M.R., Sudo, M., Stockli, D.F., Friedrich, A., Tabatabaei, S.H., 2011. Arabia-Eurasia continental collision: Insights from late Tertiary foreland-basin evolution in the Alborz Mountains, northern Iran. Geol Soc Am Bull 123, 1/2, 106-131, doi:10.1130/B30091.1.

Ballato, P., Stockli, D.F., Ghassemi, M.R., Landgraf, A., Strecker, M.R., Hassanzadeh, J., Friedrich, A., Tabatabaei, S.H., 2012. Accommodation of transpressional strain in the Arabia-Eurasia collision zone: new constraints from (U-Th)/ He thermochronology in the Alborz mountains, N Iran. Tectonics 32, doi:10.1029/2012TC003159.

ACCEPTED MANUSCRIPT

Berberian, M., King, G.C.P., 1981. Towards a paleogeography and tectonic evolution of Iran. Can. J. Earth Sci. 18, 1764-1766.

Berberian, F., Berberian, M., 1981. Tectono-Plutonic episodes in Iran. In: H.K. Gupta, and Delany, F.M. (Editor), Zagroz-Hindu Kush-Himalaya Geodynamic Evolution. American Geophysical Union & Geological Society of America, Washington, pp. 5-32.

Berberian, M., 1995. Master "blind" thrust faults hidden under the Zagros folds: active basement tectonics and surface morphotectonics. Tectonophysics 241(3-4), 193-195.

Bernet, M., 2009. A field-based estimate of the zircon fission-track closure temperature. Chem. Geol. 259(3), 181-189.

Blanc, E.J.P., Allen, M.B., Inger, S., Hassani, H., 2003. Structural styles in the Zagros simple folded zone, Iran. J. Geol. Soc. London 160: 401-412.

Brandon, M.T., 1996. Probability density plot for fission-track grain-age samples. Radiation Measurements 26(5), 663-676.

Brandon, M.T. Roden-Tice, M.K., Garver, J.I., 1998. Late Cenozoic Olympic subduction complex, Washington State, as deduced from fission track ages for detrital zircons. Am. J. Sci. 292, 565-636.

Burov, E., Jaupart, C., Guillou-Frottier, L., 2003. Ascent and emplacement of buoyant magma bodies in brittle-ductile upper crust, J. Geophys. Res. 108(B4), 2177, doi:10.1029/2002JB001904.

Cherniak, D., Watson, E., 2000. Pb diffusion in zircon, Chemical Geology, 172, pp. 5-24

ACCEPTED MANUSCRIPT

Chiu, H.Y., Zarrinkoub, M.H., Chung, S.-L., Lin, I.J., Yang, H.M., LO, C.H., Mohammadi, S.S., Khatib, M.M., 2010. Zircon U-Pb age and geochemical constraints on the magmatic and tectonic evolution in Iran. Tectonic Crossroads: Evolving Orogens of Eurasia-Africa-Arabia, Ankara, Turkey, Abstracts, 31.

Chiu, H.Y., Chung, S.L., Zarrinkoub, M.H., Mohammadi, S.S., Khatib, M.M., Iizuka, Y., 2013. Zircon U–Pb age constraints from Iran on the magmatic evolution related to Neotethyan subduction and Zagros orogeny. Lithos 162, 70-87.

Dercourt, J., Zonenshain, L.P., Ricou, L.E., Kazmin, V.G., Lepichon, X., Knipper, A.L., Grandjacquet, C., Sbortshikov, I.M., Geyssant, J., Lepvrier, C., Pechersky, D.H., Boulin, J., Sibuet, J.C., Savostin, L.A., Sorokhtin, O., Westphal, M., Bazhenov, M.L., Lauer, J.P., Bijuduval, B., 1986. Geological evolution of the tethys belt from the atlantic to the pamirs since the lias. Tectonophysics 123, 1-4, 241-315, 10.1016/0040-1951(86)90199-x.

Dimitrijevic, 1973 Geology of Kerman, Geological Survey of Iran, No. 72.

Dodson, M.H., 1973. Closure Temperature in cooling geochronological and petrological Systems. Contrib. Mineral. Petr. 40, 259-274

Ellouz-Zimmermann, N., Deville, E., Müller, C., Lallemant, S., Subhani, A. B., Tabreez, A.R., 2007. Impact of sedimentation on convergent margin tectonics: Example of the Makran accretionary prism (Pakistan). In Thrust Belts and Foreland Basins (pp. 327-350). Springer Berlin Heidelberg.

England, P., Molnar, P., 1990. Surface uplift, uplift of rocks, and exhumation of rocks. Geology 18(12), 1173-1177.

ACCEPTED MANUSCRIPT

Farley, K.A., Wolf, R. A., Silver, L.T., 1996. The effects of long alpha-stopping distances on (U-Th)/He ages. Geochim. Cosmochimim. Ac. 60(21), 4223-4229.

Farley, K.A., 2000. Helium diffusion from apatite: General behavior as illustrated by Durango fluorapatite. J. Geophys. Res. 105(B2), 2903-2914.

Farley, K.A., 2002. (U-Th)/He dating: techniques, calibrations, and applications. Reviews in Mineralogy and Geochemistry, 47(1), 819-844.

François, T., Burov E., Agard P., Meyer B., 2014, Buildup of a dynamically supported orogenic plateau: Numerical modeling of the Zagros/Central Iran case study, Geochem. Geophys. Geosyst., 15, doi:10.1002/ 2013GC005223.

Galbraith, R.F., Laslett, G.M., 1993. Statistical models for mixed fission track ages. Nuclear Tracks and Radiation Measurements 21(4), 459-470.

Gansser, A., 1955a. New aspects of the geology in Central Iran. In Fourth World Petroleum Congress, section I/A/5. Reprint (Vol. 2, pp. 280-300).

Gavillot, Y., Axen, G.J., Stockli, D.F., Horton, B.K., Fakhari, M.D., 2010. Timing of thrust activity in the High Zagros fold-thrust belt, Iran, from (U-Th)/He thermochronometry. Tectonics 29, TC4025, doi:10.1029/2009TC002484

Gleadow, A.J.W., Duddy, I.R., 1981. A natural long-term track annealing experiment for apatite. Nuclear Tracks 5(1), 169-174.

Green, P.F., Duddy, I.R. 2006. Interpretation of apatite (U–Th)/He ages and fission track ages from cratons. Earth and Planetary Science Letters,244(3), 541-547.

Green, P.F., Crowhurst, P.V., Duddy, I.R., Japsen, P., Holford, S.P. 2006. Conflicting (U–Th)/He and fission track ages in apatite: Enhanced He retention, not

ACCEPTED MANUSCRIPT

anomalous annealing behaviour. Earth and Planetary Science Letters, 250(3), 407-427.

Guest, B., Axen, G. J., Lam, P. S., Hassanzadeh, J. 2006a. Late Cenozoic shortening in the westcentral Alborz Mountains, northern Iran, by combined conjugate strike-slip and thin-skinned deformation. Geosphere 2, 35–52.

Guillot, S., Garzanti, E., Baratoux, D., Marquer, D., Mahéo, G., De Sigoyer, J., 2003. Reconstructing the total shortening history of the NW Himalaya. Geochem. Geophys. Geosyst. 4(7), doi :10.1029/2002GC000484

Hafkenscheid E., Wortel, M. J. R. and Spakman, W., 2006. Subduction history of the Tethyan region derived from seismic tomography and tectonic reconstructions. Journal of Geophysical Research, 111, B08401, doi:10.1029/2005JB003791.

Haghipour, 1974. Etude géologique de la région de Biabanak-Bafq (Iran central) : pétrologie et tectonique du socle précambrien et de sa couverture. Phd thesis, Université Scientifique et Médicale de Grenoble.

Harzhauser, M., Piller, W.E., 2007. Benchmark data of a changing sea—palaeogeography, palaeobiogeography and events in the Central Paratethys during the Miocene. Palaeogeography, Palaeoclimatology, Palaeoecology, 253(1), 8-31.

Hatzfeld, D., Molnar, P., 2010. Comparisons of the kinematics and deep structures of the Zagros and Himalaya and of the Iranian and Tibetan plateaus and geodynamic implications. Rev. Geophys. 48, RG2005, doi:10.1029/2009RG000304.

ACCEPTED MANUSCRIPT

Hessami, K., Koyi, H.A., Talbot, C.J., Tabasi, H., Shabanian, E., 2001. Progressive unconformities within an evolving foreland fold-thrust belt, Zagros Mountains. J. Geol. Soc. 158, 969-981.

Homke, S., Vergés, J., van der Beek, P.A., Fernàndez, M., Saura, E., Barbero, L., Badics, B., Labrin, E., 2010. Insights in the exhumation history of the NW Zagros from bedrock and detrital apatite fission-track analysis: evidence for a long-lived orogeny. Basin Res. 22, 5, 659–680, doi: 10.1111/j.1365-2117.2009.00431.x.

Hurford, A.J., & Green, P.F. (1982). A users' guide to fission track dating calibration. Earth Planet. Sci. Lett. 59(2), 343-354.

Hurford, A.J., Hammerschmidt, K., 1985. 40Ar39Ar and K/Ar dating of the Bishop and Fish Canyon Tuffs: Calibration ages for fission-track dating standards. Chemical Geology: Isotope Geoscience section 58(1), 23-32.

Hurford, A. J., 1986. Cooling and uplift patterns in the Lepontine Alps South Central Switzerland and an age of vertical movement on the Insubric fault line. Contributions to mineralogy and petrology, 92(4), 413-427.

Jackson, M.P.A., Cornelius, R.R., Craig, C.H., Gansser, A., Stöcklin, J., Talbot, C.J., 1990. Salt Diapirs of the Great Kavir, Central Iran. Geological Society of America Memoir 177, 1-139.

Jackson, J., 2011. Review of: Tectonic and Stratigraphic Evolution of the Zagros and Makran During the Mesozoic–Cenozoic. Geological Society Special Publication 330. Geological Magazine, 148 (5-6). p. 1018

Jahangiri, A., 2007. Post-collisional Miocene adakitic volcanism in NW Iran: Geochemical and geodynamic implications. J. Asian Earth Sci. 30(3-4): 433-

ACCEPTED MANUSCRIPT

447.

Jolivet, L., Faccenna, C., 2000. Mediterranean extension and the Africa-Eurasia collision. Tectonics 19(6): 1095-1106.

Kargaranbafghi, F., Neubauer, F., Genser, J., 2010. Mesozoic and Eocene ductile deformation of western Central Iran: from Cimmerian collisional orogeny to Eocene extension and exhumation. In EGU General Assembly Conference Abstracts (Vol. 12, p. 6268).

Karagaranbafghi, F., Foeken, J.P.T., Guest, B., Stuart, F.M., 2012. Cooling history of the Chapedony metamorphic core complex, Central Iran: Implications for the Eurasia–Arabia collision. Tectonophysics 524, 100-107.

Khadivi, S., Mouthereau, F., Barbarand, J., Adatte, T., Lacombe, O., 2012. Constraints on paleodrainage evolution induced by uplift and exhumation on the southern flank of the Zagros-Iranian Plateau, J. Geol. Soc. 169, no. 1, doi:10.1144/0016-76492011-031.

Kukowski, N., Neugebauer, H.J., 1990. On the ascent and emplacement of granitoid magma bodies dynamic-thermal numerical models. Geologische Rundschau, 79(2), 227-239.

Lacombe, O., Mouthereau, F., Kargar, S., Meyer, B., 2006. Late Cenozoic and modern stress fields in the western Fars (Iran): Implications for the tectonic and kinematic evolution of central Zagros. Tectonics 25, TC1003, doi:10.1029/2005TC001831.

ACCEPTED MANUSCRIPT

Liu-Zeng, J., Tapponnier, P., Gaudemer, Y., Ding, L., 2008. Quantifying landscape differences across the Tibetan plateau: Implications for topographic relief evolution, J. Geophys. Res. 113, F04018, doi:10.1029/2007JF000897.

McQuarrie, N., Stock, J.M., Verdel, C., Wernicke, B.P., 2003. Cenozoic evolution of Neotethys and implications for the causes of plate motions. Geophys. Res. Lett. 30(20), 2036, doi:10.1029/2003GL017992.

McQuarrie, N., 2004. Crustal scale geometry of the Zagros fold-thrust belt, Iran. J. Struct. Geol., 26(3): 519-535.

McQuarrie, N., van Hinsbergen, D.J., 2013. Retrodeforming the Arabia-Eurasia collision zone: Age of collision versus magnitude of continental subduction. Geology 41(3), 315-318.

Meyer, B., Tapponnier, P., Bourjot, L., Metivier, F., Gaudemer, Y., Peltzer, G., Shunmin, G., Zhitai, C., 1998. Crustal thickening in Gansu-Qinghai, lithospheric mantle subduction, and oblique, strike-slip controlled growth of the Tibet plateau. Geophys. J. Int. 135(1), 1-47.

Meyer, B., Mouthereau, F., Lacombe, O., Agard, P., 2006. Evidence of Quaternary activity along the Deshir Fault: implication for the Tertiary tectonics of Central Iran. Geophys J. Int. 164(1), 192-201.

Molinaro, M., Zeyen, H., Laurencin, X., 2005b. Lithospheric structure underneath the SE Zagros Mountains, Iran: recent slab break-off? Terra Nova 25, 1, 1-6.

Molnar, P., England, P., Martinod, J., 1993. Mantle dynamics, uplift of the Tibetan Plateau, and the Indian monsoon. Reviews of Geophysics 31(4), 357-396.

ACCEPTED MANUSCRIPT

Moritz, R., Ghazban, F., Singer, B.S., 2006. Eocene gold ore formation at Muteh, Sanandaj-Sirjan Tectonic Zone, Western Iran: a result of late-stage extension and exhumation of metamorphic basement rocks within the Zagros Orogen. Econ. Geol. 101(8), 1497-1524.

Morley, C.K., Kongwung, B., Julapour, A.A., Abdolghafourian, M., Hajian, M., Waples, D., Warren, J., Otterdoom, H., Srisuriyon, K., Kazemi, H., 2009. Structural development of a major late Cenozoic basin and transpressional belt in central Iran: The Central Basin in the Qom-Saveh area. Geosphere 5(4), 325-362.

Mouthereau, F., Lacombe, O., Meyer, B., 2006. The Zagros Folded Belt (Fars, Iran): Constraints from Topography and Critical Wedge Modelling. Geophys. J. Int. 165, 336-356.

Mouthereau, F., Tensi, J., Bellahsen, N., Lacombe, O., De Boisgrollier, T., Kargar, S., 2007b. Tertiary sequence of deformation in a thin-skinned/thick-skinned collision belt: the Zagros Folded Belt (Fars, Iran). Tectonics 26, TC5006, doi:10.1029/2007TC002098.

Mouthereau, F., Lacombe, O., Vergés, J., 2012. Building the Zagros collisional orogen: timing, strain distribution and the dynamics of Arabia/Eurasia plate convergence. Tectonophysics 532, 27-60.

Nadimi, A., 2007. Evolution of the Central Iranian basement. Gondwana Res. 12(3): 324-333.

ACCEPTED MANUSCRIPT

Naeser, C.W., Fleischer, R.L., 1975. Age of the apatite at Cerro de Mercado, Mexico: A problem for fission- track annealing corrections. Geophys. Res. Lett. 2(2), 67-70.

Omrani, J., 2008. The geodynamic evolution of Zagros: Tectonic and petrological constraints from the internal zones. Unpublihed PhD Thesis, Université. Pierre-et-Marie-Curie, Paris.

Omrani, J., Agard, P., Whitechurch, H., Benoit, M., Prouteau, G., Jolivet, L., 2008. Arc-magmatism and subduction history beneath the Zagros Mountains, Iran: a new report of adakites and geodynamic consequences, Lithos 106, 380-398, doi:10.1016/j.lithos.2008.09.008.

Patriat, P., Achache, J., 1984. India-Eurasia chronology has implications for crustal shortening and driving mechanism of plates. Nature 311, 615-621, doi:10.103/311615a0

Petford, N., Cruden, A.R., McCaffrey, K.J.W., Vigneresse, J.L., 2000. Granite magma formation, transport and emplacement in the Earth's crust. Nature 408(6813), 669-673.

Reiners, P.W., Farley, K.A., 2001. Influence of crystal size on apatite (U–Th)/He thermochronology: an example from the Bighorn Mountains, Wyoming.Earth and Planetary Science Letters, 188(3), 413-420.

Reiners, P.W., Brandon, M.T., 2006. Using thermochronology to understand orogenic erosion. Annu. Rev. Earth Pl. Sci. 34, 419-466.

ACCEPTED MANUSCRIPT

Rezaeian, M.A. Carter, N., Hovius, Allen, M.B., 2012. Cenozoic exhumation history of the Alborz Mountains, Iran: New constraints from low-temperature chronometry, Tectonics 31, TC2004, doi:10.1029/2011TC002974.

Reuter, M., Piller, W.E., Harzhauser, M., Mandic, O., Berning, B., Rogl, F., Kroh, A., Aubry, M.-P., Wielandt-Schuster, U., Hamedani, A., 2009. The Oligo-/Miocene Qom Formation (Iran): evidence for an early Burdigalian restriction of the Tethyan Seaway and closure of its Iranian gateways. Int. J. Earth Sci. 98, 3, 627–650, 10.1007/s00531-007-0269-9.

Ricou, L.-E., Braud, J., Brunn, J.H., 1977. Le Zagros, Livre à la mémoire de A.F. de Lapparent. Société géologique de France, Paris, pp. 33-52.

Rohrmann, A., Kapp, P., Carrapa, B., Reiners, P.W., Guynn, J., Ding, L., Heizler, M., 2012. Thermochronologic evidence for plateau formation in central Tibet by 45 Ma. Geology 40(2), 187-190.

Royden, L. H., Burchfiel, B.C., King, R.W., Wang, E., Chen, Z, Shen, F., Liu Y. 1997. Surface Deformation and Lower Crustal Flow in Eastern Tibet. Science 276(5313), 788-790.

Schröder, J.W., 1944. Essai sur la structure de l'Iran. Eclogae geologicae Helvetiae, 37: 37-81.

Şengör, A.C., 1984. The Cimmeride orogenic system and the tectonics of Eurasia. Geol. Soc. Am. Special Papers, 195, 1-74.

Sengör, A.M.C., 1990. A new model for the late Palaeozoic-Mesozoic tectonic evolution of Iran and implications for Oman. Geol. Soc, London, Spec. Pub. 797-831.

ACCEPTED MANUSCRIPT

Shahabpour, J., 2005. Tectonic evolution of the orogenic belt in the region located between Kerman and Neyriz. J. Asian Earth Sci. 24(4): 405-417.

Stampfli, G.M., Borel, G.D., 2002. A plate tectonic model for the Paleozoic and Mesozoic constrained by dynamic plate boundaries and restored synthetic oceanic isochrons. Earth and Planetary Science Letters 196, 7–33.

Stewart, R.J., Brandon, M.T., 2004. Detrital-zircon fission-track ages for the "Hoh Formation": Implications for late Cenozoic evolution of the Cascadia subduction wedge. Geol. Soc. Am. Bull. 116(1-2), 60-75.

Stöcklin, J., 1968. Structural history and tectonics of Iran; a review. AAPG Bull. 52, 7, 1229-1258.

Tapponnier, P., Zhiqin, X., Roger, F., Meyer, B., Arnaud, N., Wittlinger, G., Jingsui, Y., 2001. Oblique stepwise rise and growth of the Tibet Plateau. Science 294(5547), 1671-1677.

van der Beek, P., Van Melle J., Guillot, S., Pêcher A., Reiners P.W., Nicolescu, S., Latif, M. 2009, Eocene Tibetan plateau remnants preserved in the northwest Himalaya, Nature Geosci. doi: 10.1038/NGEO503

van Hunen, J., Allen, M.B., 2011. Continental collision and slab break-off: A comparison of 3-D numerical models with observations. Earth Planet. Sci. Lett., 302(1), 27-37.

Verdel, C., Wernicke, B.P., Ramezani, J., Hassanzadeh, J., Renne, P.R., Spell, T.L., 2007. Geology and thermochronology of Tertiary Cordilleran-style metamorphic core complexes in the Saghand region of central Iran. Geol. Soc. Am. Bull. 119, 7/8, 961-977.

ACCEPTED MANUSCRIPT

Vergés, J., Saura, E., Casciallo, E., Fernàndez, M., Villaseñor, A., Jiménez-Munt, I., García-Castellanos, D., 2011. Crustal-scale cross-sections across the NW Zagros belt: Implications for the Arabian margin reconstruction. Geol. Mag. 148, 739-761, doi:10.1017/S001676811000331.

Vernant, P., Nilforoushan, F., Hatzfeld, D., Abbassi, M.R., Vigny, C., Masson, F., Nankali, H., Martinod, J., Ashtiani, A., Bayer, R., Tavakoli, F., Chéry, J., 2004. Present-day crustal deformation and plate kinematics in the Middle East constrained by GPS measurements in Iran and northern Oman. Geophys. J. Int. 157, 381-398.

Vincent, S.J., Allen, M.B., Ismail-Zadeh, A.D., Flecker, R., Foland, K.A., Simmons, M.D., 2005. Insights from the Talysh of Azerbaijan into the Paleogene evolution of the South Caspian region. Geol. Soc. Am. Bull. 117, 11/12, 1513–1533, doi: 10.1130/B25690.1.

Weinberg, R.F., Podladchikov, Y., 1994. Diapiric ascent of magmas through power law crust and mantle. J. Geophys. Res.: Solid Earth (1978-2012), 99(B5), 9543-9559.

Whitechurch, H., Omrani, J., Agard, P., Humbert, H., Montigny, R.L., Jolivet, L., 2013. Evidence for a Paleocene-Eocene Back-Arc to Arc evolution at the foot of the Eurasian margin (Kermanshah ophiolite, SW Iran): implications for regional geodynamics and obduction. Lithos

Willett, S.D., Brandon, M.T., 2013. Some analytical methods for converting thermochronometric age to erosion rate, Geochem. Geophys. Geosyst. 14, 209–222, doi:10.1029/2012GC004279.

ACCEPTED MANUSCRIPT

Wrobel-Daveau, 2011. From the rifting to the current collision, vertical movements and propagation of the deformation in the Zagros Belt, Iran. Insights from section balancing and detrital low temperature thermochronology. Thèse Université de Cergy-Pontoise

ACCEPTED MANUSCRIPT

ACCEPTED MANUSCRIPT

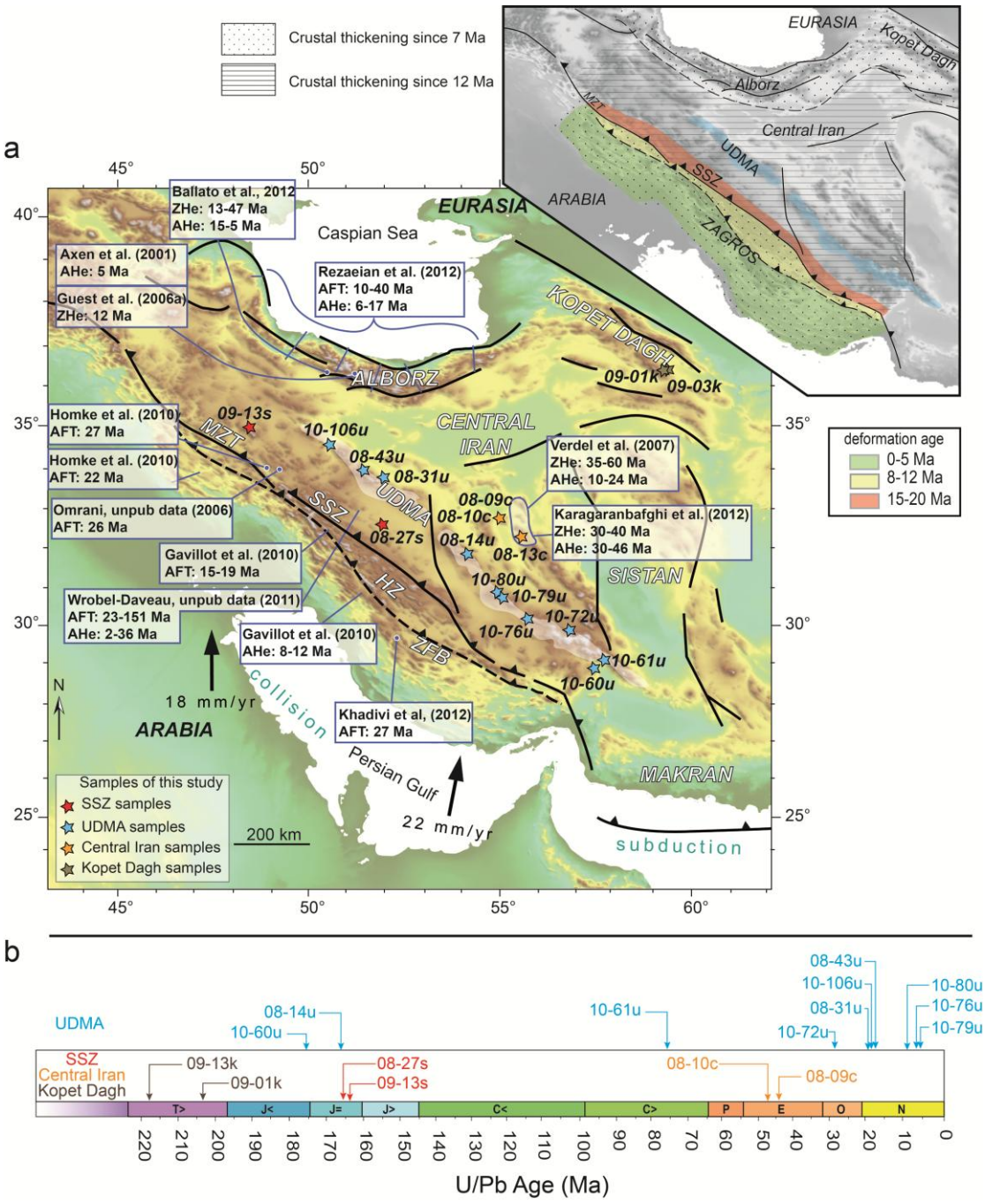

Fig. 1

ACCEPTED MANUSCRIPT

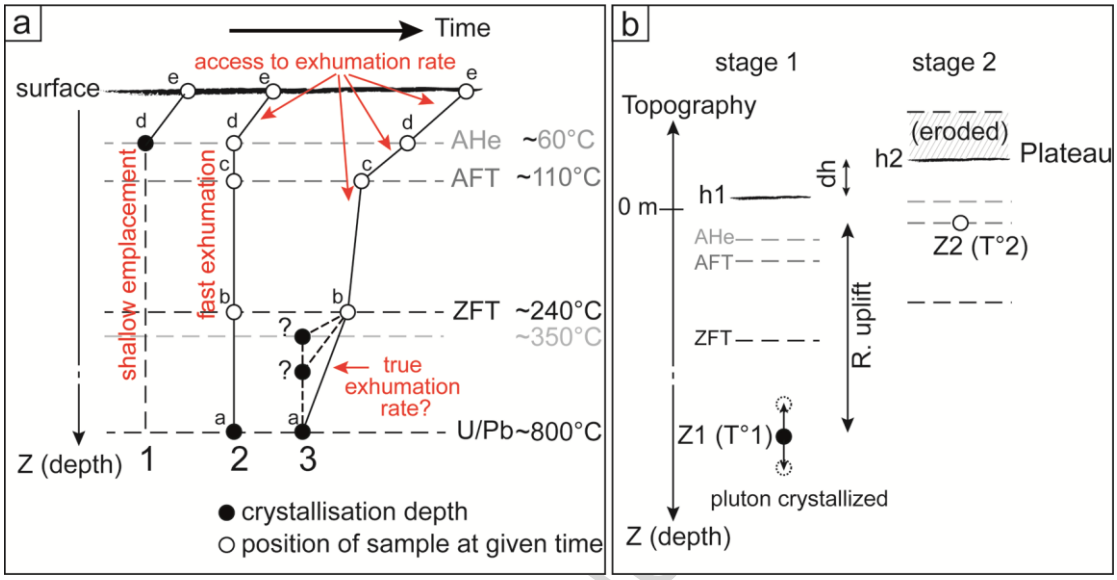

Fig. 2

ACCEPTED MANUSCRIPT

ACCEPTED MANUSCRIPT

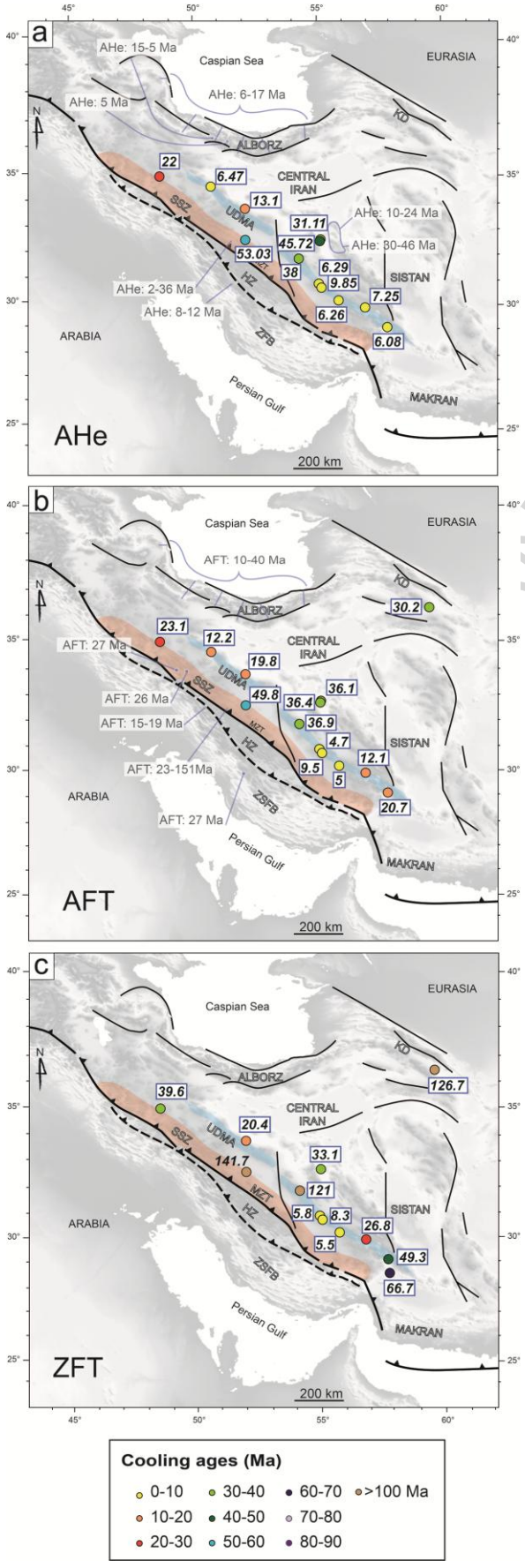

Fig. 3

ACCEPTED MANUSCRIPT

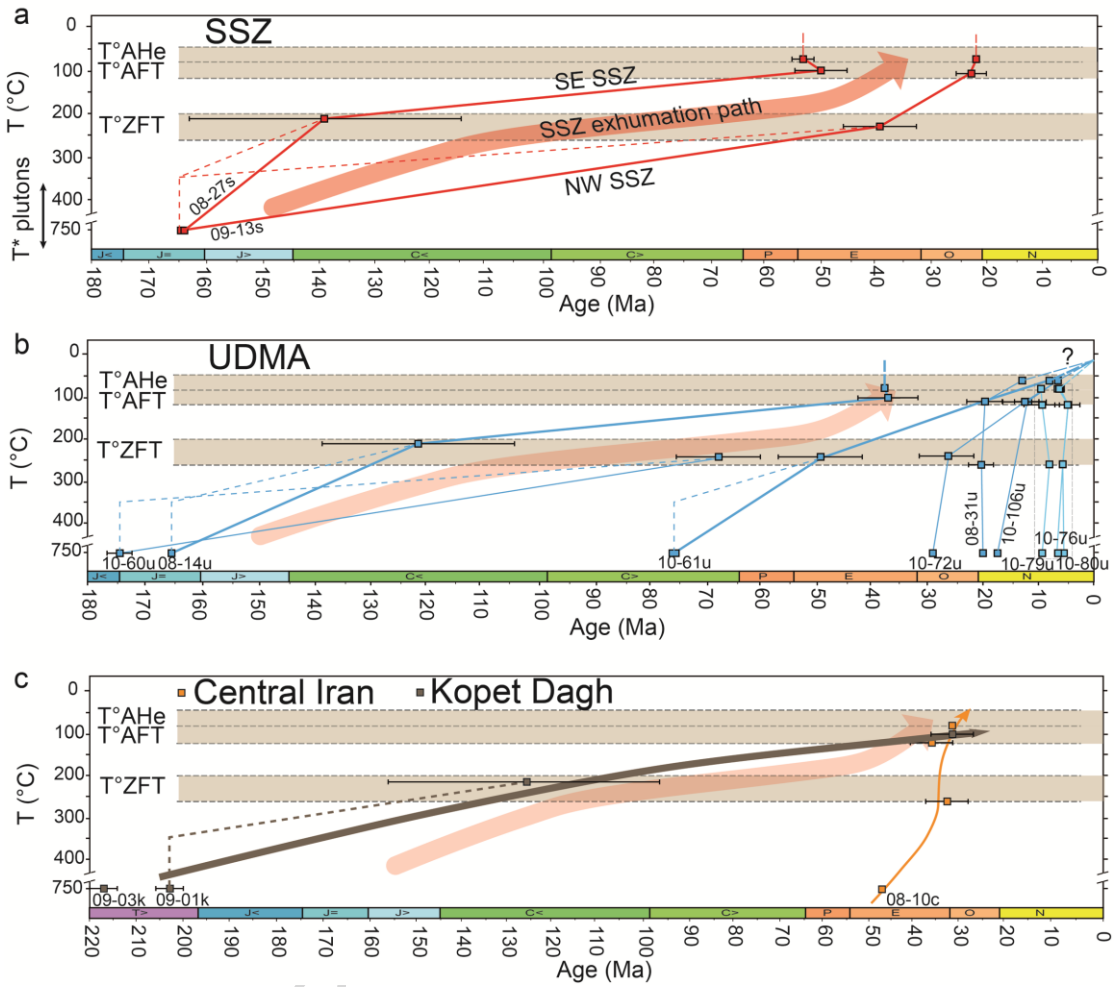

Fig. 4

ACCEP

ACCEPTED MANUSCRIPT

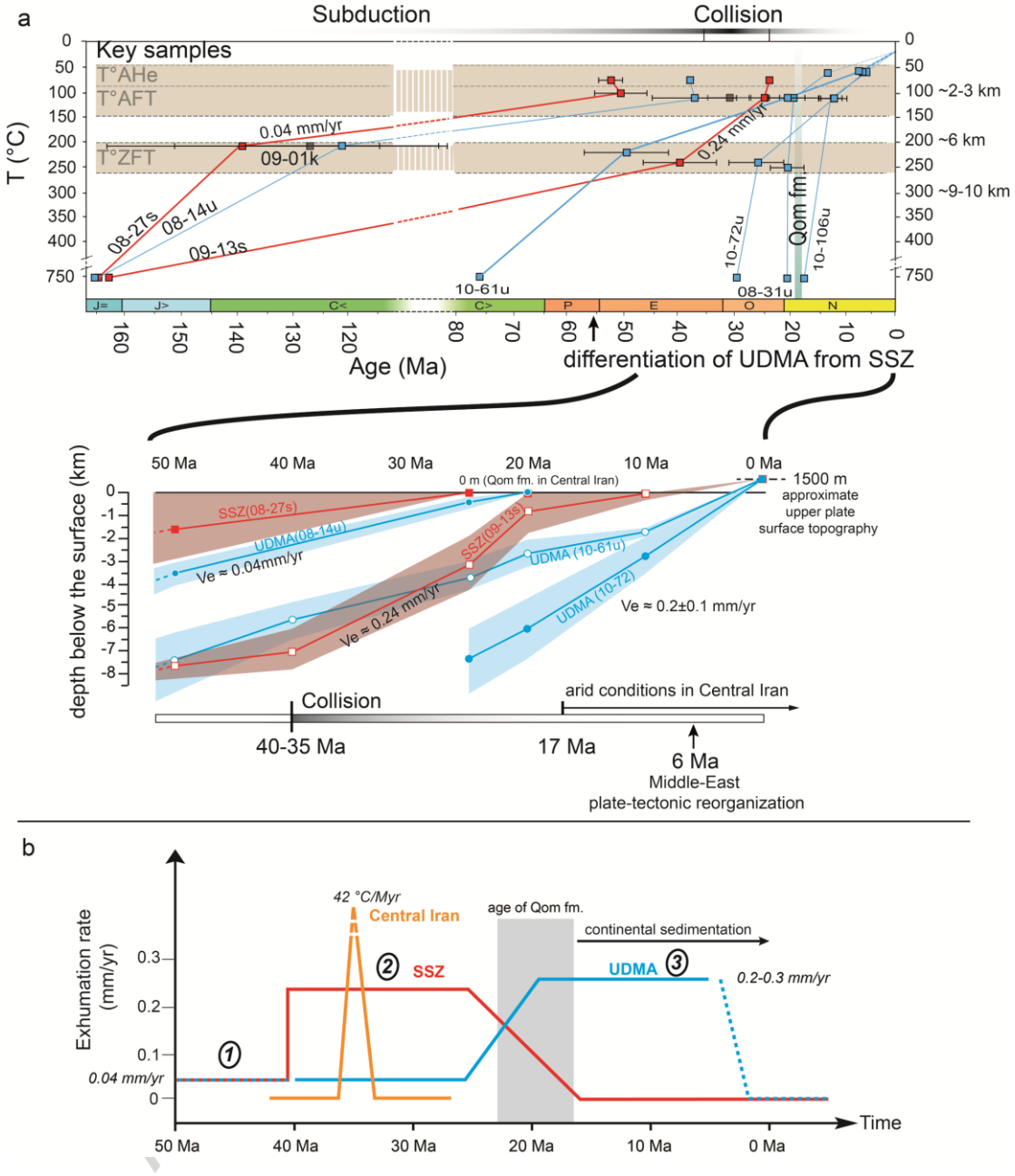

Fig. 5

ACCEPTED MANUSCRIPT

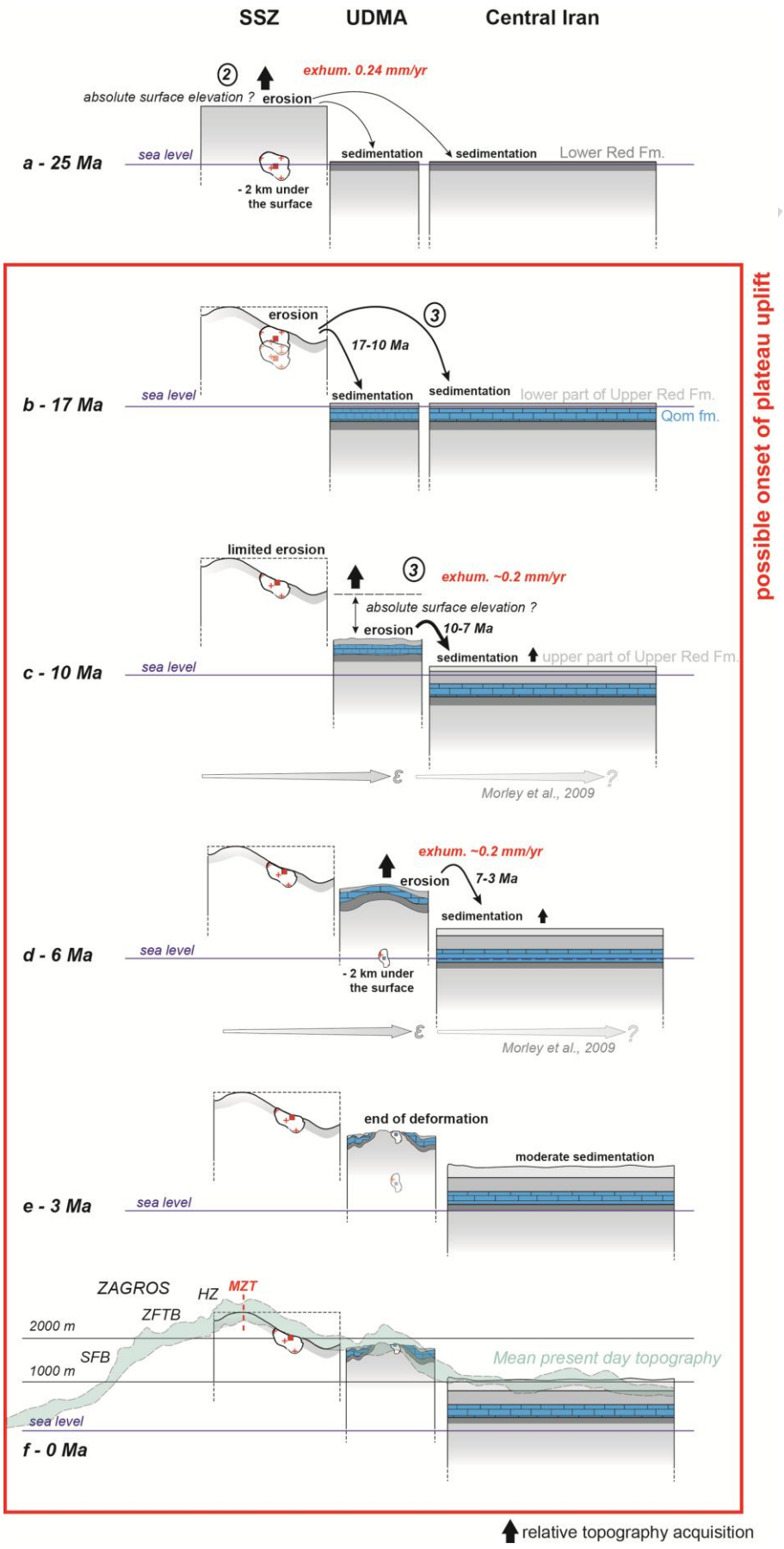

Fig. 6

ACCEPTED MANUSCRIPT

Table 1

Sample	Longitude (°E)	Latitude (°N)	Elevation (m)	Rocks type	SiO2 (%)	Zircon	Apatite	U/Pb Age	± 2σ
SSZ									
09-13s	48° 26' 38"	34° 45' 28"	2187	leucogranite		-	-	165.1	2.0
08-27s	51° 55' 06"	32° 18' 54"	1938	granite	67.95	-	-	164.6	2.1
UDMA									
08-14u	54° 07' 26"	31° 35' 32"	2568	granite	67.72	-	-	166.1	1.5
08-31u	51° 55' 19"	33° 29' 28"	1727	granite	65.56	-	-	20.2	0.3
10-60u	57° 26' 02"	28° 43' 27"	1384	granite	75.18	-	×	175.2	1.8
10-61u	57° 40' 07"	28° 55' 02"	1398	gabbro	52.20	-	-	76.6	0.9
10-72u	56° 47' 00"	29° 40' 40"	2369	diorite	56.17	-	-	29.3	0.3
10-76u	55° 42' 55"	29° 57' 33"	2376	microdiorite	65.07	-	-	6.5	0.1
10-79u	55° 00' 29"	30° 28' 28"	2337	granodiorite	62.46	-	-	9.4	0.1
10-80u	54° 55' 16"	30° 35' 56"	2578	granodiorite	64.25	-	-	5.4	0.1
10-106u	50° 30' 39"	34° 19' 45"	1298	granodiorite	60.25	-	-	17.4	0.2
Central Iran									
08-10c	54° 58' 29"	32° 29' 01"	1042	gneiss	74.03	-	-	47.5	0.4
Kopet Dagh									
09-01k	59° 24' 25"	36° 08' 57"	1047	granodiorite	65.63	-	-	203.3	2.6
09-03k	59° 33' 27"	36° 16' 50"	1016	diorite	60.73	-	×	218.7	2.2

ACCEPTED MANUSCRIPT

Table 2

Sample	Length (μm)	Width (μm)	^{4}He (mol/g)	U (mol)	Th (mol)	Ft	Age (Ma)	Std dev
SSZ								
09-13s (a)	300	150	2.15×10^{-14}	7.15×10^{-15}	3.60×10^{-13}	0.815	18.90	0.13
09-13s (b)	310	160	3.87×10^{-14}	5.21×10^{-12}	3.32×10^{-13}	0.825	29.96	0.29
09-13s (c)	330	250	4.93×10^{-14}	3.24×10^{-14}	1.42×10^{-12}	0.875	20.14	0.19
09-13s (d)	250	180	1.39×10^{-14}	1.07×10^{-14}	2.08×10^{-13}	0.832	19.22	0.34
							22.06	**0.24**
08-27s (a)	230	170	2.91×10^{-14}	6.72×10^{-13}	9.79×10^{-14}	0.639	50.95	0.39
08-27s (c)	250	150	3.81×10^{-14}	7.82×10^{-13}	1.15×10^{-13}	0.665	54.91	0.51
08-27s (d)	230	160	7.13×10^{-15}	1.55×10^{-13}	4.39×10^{-14}	0.629	53.24	1.20
							53.03	**0.70**
UDMA								
08-14u (a)	130	80	5.44×10^{-15}	1.09×10^{-13}	1.09×10^{-13}	0.651	48.29	1.30
08-14u (b)	110	100	6.39×10^{-15}	2.11×10^{-13}	1.14×10^{-13}	0.692	30.25	0.27
08-14u (d)	140	100	9.66×10^{-15}	9.60×10^{-14}	9.19×10^{-14}	0.687	35.46	2.74
							38	**1.40**
08-31u (a)	200	90	4.32×10^{-15}	1.02×10^{-13}	5.75×10^{-13}	0.698	12.63	0.20
08-31u (b)	190	75	2.72×10^{-15}	5.35×10^{-15}	4.67×10^{-13}	0.646	12.79	0.19
08-31u (c)	175	90	5.36×10^{-15}	3.73×10^{-15}	8.23×10^{-13}	0.687	13.77	0.24
08-31u (d)	170	100	4.85×10^{-15}	5.61×10^{-15}	6.89×10^{-13}	0.709	13.16	0.13
							13.09	**0.19**
10-61u (a)	250	130	1.62×10^{-15}	1.87×10^{-13}	4.05×10^{-13}	0.697	6.58	0.24
10-61u (b)	200	140	4.54×10^{-15}	4.65×10^{-13}	7.80×10^{-13}	0.588	5.84	0.40
10-61u (d)	130	100	2.16×10^{-15}	2.78×10^{-13}	5.42×10^{-13}	0.626	5.81	0.29
							6.08	**0.31**
10-72u (a)	360	110	9.37×10^{-15}	4.46×10^{-13}	2.87×10^{-12}	0.752	8.74	0.08
10-72u (b)	200	130	6.05×10^{-15}	4.29×10^{-13}	2.12×10^{-12}	0.764	6.72	0.05
10-72u (c)	200	160	5.21×10^{-15}	3.99×10^{-13}	2.58×10^{-12}	0.794	5.43	0.05
10-72u (d)	150	100	4.69×10^{-15}	2.91×10^{-13}	1.54×10^{-12}	0.697	8.12	0.07
							7.25	**0.06**
10-76u (a)	130	60	2.54×10^{-16}	2.75×10^{-14}	1.06×10^{-13}	0.558	6.82	0.47
10-76u (b)	150	100	5.92×10^{-16}	4.61×10^{-14}	2.35×10^{-13}	0.697	6.58	0.24
10-76u (c)	120	70	2.84×10^{-16}	1.96×10^{-14}	1.94×10^{-13}	0.588	5.84	0.40
10-76u (d)	150	75	3.98×10^{-16}	3.46×10^{-14}	2.19×10^{-13}	0.623	5.81	0.29
							6.26	**0.25**
10-79u (a)	300	110	3.76×10^{-15}	1.78×10^{-13}	8.28×10^{-13}	0.764	10.39	0.20
10-79u (b)	250	125	2.71×10^{-15}	1.45×10^{-13}	7.07×10^{-13}	0.781	8.78	0.11
10-79u (c)	190	130	2.81×10^{-15}	1.36×10^{-13}	6.40×10^{-13}	0.775	9.94	0.14
10-79u (d)	330	120	4.39×10^{-15}	2.16×10^{-13}	9.04×10^{-13}	0.782	10.28	0.08
							9.85	**0.13**
10-80u (a)	325	140	4.43×10^{-15}	4.32×10^{-13}	1.03×10^{-12}	0.799	6.44	0.09
10-80u (b)	375	175	8.69×10^{-15}	8.37×10^{-13}	1.97×10^{-12}	0.836	6.27	0.07
10-80u (c)	360	160	6.33×10^{-15}	6.11×10^{-13}	1.62×10^{-12}	0.822	6.09	0.09
10-80u (d)	430	160	7.42×10^{-15}	6.88×10^{-13}	1.78×10^{-12}	0.826	6.35	0.07
							6.29	**0.08**
10-106u (a)	190	90	3.37×10^{-17}	3.28×10^{-14}	2.59×10^{-14}	0.676	5.37	3.00
10-106u (b)	130	80	3.39×10^{-16}	2.92×10^{-15}	1.06×10^{-13}	0.634	9.83	0.59
10-106u (c)	150	120	3.21×10^{-16}	2.67×10^{-15}	2.24×10^{-13}	0.729	4.40	0.29
10-106u (d)	100	75	1.24×10^{-16}	2.32×10^{-15}	8.34×10^{-14}	0.594	5.62	0.80
							6.47	**0.99**
Central Iran								
08-10c (a)	230	170	7.67×10^{-14}	2.51×10^{-12}	5.04×10^{-13}	0.823	27.62	0.18
08-10c (b)	350	140	1.13×10^{-13}	3.01×10^{-12}	7.38×10^{-13}	0.809	33.99	0.20
08-10c (c)	250	150	1.04×10^{-13}	2.60×10^{-12}	2.15×10^{-12}	0.806	32.56	0.44
08-10c(d)	230	160	1.27×10^{-13}	3.77×10^{-12}	1.04×10^{-12}	0.814	30.27	0.16
							31.11	**0.24**

ACCEPTED MANUSCRIPT

Table 3

Sample	No of grains	ρ_s (N_s) $\times 10^5$ cm^{-2}	ρ_i (N_i) $\times 10^5$ cm^{-2}	$P(\chi^2)$ (%)	Disp (%)	Pooled Age (Ma)	2σ (Ma)
SSZ							
09-13s	31	2.05 (341)	8.83 (1467)	12.6	20.4	23.1	3
08-27s	22	17.5 (787)	35.1 (1574)	100	0	49.8	4.8
UDMA							
08-14u	24	3.51 (219)	9.51 (593)	100	0	36.9	5.5
08-31u*	20	1.32 (71)	6.64 (358)	100	0.1	19.8	5
10-61u*	19	1.16 (61)	5.65 (296)	100	0.1	20.7	5.5
10-72u*	29	0.24 (83)	6.85 (690)	98.6	0.3	12.1	2.8
10-76u*	16	0.18 (7)	2.59 (154)	99.9	0	4.7	2
10-79u*	27	0.26 (51)	2.74 (544)	100	0.1	9.4	2.8
10-80u*	32	0.73 (40)	3.70 (857)	93	0.4	4.7	1.5
10-106u*	10	0.29 (19)	1.87 (155)	100	0	12.3	5
Central Iran							
08-10c	25	6.97 (654)	19.1 (1789)	80.6	1.4	36.4	3.6
Kopet Dagh							
09-01k	18	3.44 (303)	11.4 (1008)	100	0	30.1	4

Table 4

Sample	No of grains	ρ_s (N_s) $\times 10^6$ cm^{-2}	ρ_i (N_i) $\times 10^6$ cm^{-2}	$P(\chi^2)$ (%)	Disp (%)	Pooled Age (Ma)	2σ (Ma)
SSZ							
09-13s	31	4.1 (508)	2.09 (259)	100	0	39.5	6.5
08-27s	14	7.79 (796)	1.01 (112)	100	0	141.1	26
UDMA							
08-14u	22	8.9 (1711)	1.47 (282)	100	0	120.8	17
08-31u	20	3.21 (900)	3.16 (886)	80.2	0.7	20.4	2.5
10-60u	12	22.7 (1351)	6.88 (409)	93.2	0.2	66.7	9
10-61u	20	2.71 (619)	1.11 (254)	100	0	49.2	8
10-72u	18	5.06 (1016)	3.84 (770)	21.5	3.9	26.8	3.3
10-76u	24	0.93 (465)	2.56 (1718)	99.9	0.1	5.5	0.7
10-79u	25	1.22 (708)	3.01 (1746)	97.9	0.2	8.3	0.9
10-80u*	24	0.85 (214)	2.95 (746)	2.5	29.6	5.8	1
Central Iran							
08-10c	15	6.26 (980)	1.67 (595)	34.4	6.7	33.1	4.3
Kopet Dagh							
09-03k	10	8.54 (475)	1.35 (75)	100	0	126.7	30

ACCEPTED MANUSCRIPT

Figure captions

Figure 1.

Sampling locations:

a) Topographic map showing the main structures within the Arabia-Eurasian convergence zone and sample locations. Blue frames show available low temperature thermochronology data in the literature (data from, Axen et al., 2001; Omrani, unpub data, 2008; Verdel et al., 2007; Guest et al., 2006a; Gavillot et al., 2010; Homke et al., 2010; Karagaranbafghi et al., 2012; Khadivi et al., 2012; Wrobel-Daveau, unpub data, 2011; Ballato et al., 2012; Rezaeian et al., 2012. Black arrows indicate convergence rates of Arabia with respect to Eurasia (from Vernant et al., 2004). Inset: simplified structural map showing the extension of crustal thickening over the last 12 and 7 Myr across the Arabia-Eurasia collision, as suggested by Allen et al. (2004).

b) Ages of the selected plutonic samples (from Chiu et al., 2010; see Table 1 for details).

Figure 2.

a) Cartoon illustrating the various possible interpretations of cooling ages of plutons emplaced at different depths, assuming a constant geothermal gradient. In the first two cases, the overlap of ages is ambiguous and may indicate either shallow emplacement of the pluton (1) or rapid exhumation (2). In the third case, the different cooling ages reveal the effective exhumation and provide informative temperature-time paths

b) Cartoon recalling that surface uplift (dh) is equal to rock uplift (R. uplift) minus exhumation (i.e., erosion; England and Molnar 1990). Exhumation corresponds here to the net difference between (h2+Z2) and (h1+Z1), where h and Z are positive and

ACCEPTED MANUSCRIPT

negative, respectively.

Figure 3.

Low-temperature thermochronology data and location of calculated ages: **a)** AHe, **b)** AFT and **c)** ZFT. See caption of Figure 1 for references of published ages.

Figure 4.

Cooling paths for the (a) SSZ, (b) UDMA, (c) Central Iran and Kopet Dagh. The closure temperature for each sample is calculated as a function of exhumation rate (see Reiners and Brandon, 2006). Dashed lines represents minimal exhumation rates (see § 3.3).

Figure 5.

a) Cooling paths of key samples (see text). The depth range is calculated for a thermal geotherm of 30°/km. The age of the Qom Formation is indicated (Qom fm.) and Depth-time position of these key samples (irrespective of their exact elevation) at 50, 25, 20, 13 and 0 Ma. Error envelopes incorporate all associated uncertainties (i.e., analytical standard deviations, ambiguities associated with early exhumation paths; see chapter 3.3).

b) Evolution of exhumation rate between 50 and 0 Ma for the SSZ, UDMA and Central Iran. The number corresponds to the different stage of exhumation history subsequently shown in the Fig.6.

Figure 6.

Tentative relative topographic reconstruction over the last 50 Myr along a NE-SW

ACCEPTED MANUSCRIPT

traverse. Each time step is set against the evolution of the Arabia-Eurasia convergence (see text). The sedimentary record from the Central Iranian basin is schematized from Morley et al., (2009). The present day topography of Central Zagros is represented by the blue line in the panel 6.f (0 Ma).

Table 1: Sample locations, Rocks type and U/Pb Ages

Table 2: Analytical data for apatite (U-Th)/He age determination

Table 3: Apatite fission track analytical data. The stars represent the sample with low U concentration

Table 4: Zircon fission track analytical data. The stars represent the sample with low U concentration

ACCEPTED MANUSCRIPT

ACCEPTED MANUSCRIPT

Highlights

. first thermochronological data with a vast coverage of the Iranian plateau

. combination of low-temperature thermochronology data, apatite (U-Th)/He, apatite and zircon fission-track dating

. exhumation migrated to the NE (UDMA) after ~20 Ma, at the same time as towards the SW (external Zagros)

ACCEPTED MANUSCRIPT